The *Mycobacterium tuberculosis* Pup-proteasome system regulates nitrate metabolism through an essential protein quality control system

Samuel H. Becker[1], Jordan B. Jastrab[1,2], Avantika Dhabaria[3], Catherine T. Chaton[4], Jeffrey S. Rush[4], Konstantin V. Korotkov[4], Beatrix Ueberheide[3], and K. Heran Darwin[1*]

[1]Department of Microbiology, New York University School of Medicine, 430 E. 29th Street, Suite 312, New York, NY 10016, USA

[2]Current address: Department of Medicine, Brigham and Women's Hospital, Boston, MA 02115, USA

[3]Proteomics Laboratory, Division of Advanced Research Technologies, New York University School of Medicine, 430 E. 29th Street, Suite 860, New York, NY 10016

[4]Department of Molecular and Cellular Biochemistry, University of Kentucky, 741 S. Limestone Street, Lexington, KY 40536, USA

*Corresponding author: heran.darwin@med.nyu.edu

Classification: Biological Sciences: Microbiology

Keywords: *Mycobacterium tuberculosis*, proteasome, nitrate, chaperonins

ABSTRACT

The human pathogen *Mycobacterium tuberculosis* (*M. tuberculosis*) encodes a proteasome that carries out regulated degradation of bacterial proteins. It has been proposed that the proteasome contributes to nitrogen metabolism in *M. tuberculosis,* although this hypothesis had not been tested. Upon assessing *M. tuberculosis* growth in several nitrogen sources, we found that a mutant strain lacking the *Mycobacterium* proteasomal activator Mpa was unable to use nitrate as a sole nitrogen source due to a specific failure in the pathway of nitrate reduction to ammonium. We found that the robust activity by the nitrite reductase complex NirBD depended on expression of the *groEL*/*groES* chaperonin genes, which are regulated by the repressor HrcA. We identified HrcA as a likely proteasome substrate, and propose that the degradation of HrcA is required for the full expression of chaperonin genes. Furthermore, our data suggest that degradation of HrcA, along with numerous other proteasome substrates, is enhanced during growth in nitrate to facilitate the de-repression of the chaperonin genes. Importantly, growth in nitrate is the first example of a specific condition that reduces the steady-state levels of numerous proteasome substrates in *M. tuberculosis*.

SIGNIFICANCE STATEMENT

The proteasome is required for the full virulence of *M. tuberculosis*. However, the extent of its role as a regulator of bacterial physiology remains unclear. In this work, we demonstrate a novel function of the proteasome system in maintaining the expression of essential chaperonin genes. This activity by the proteasome is required for *M. tuberculosis* to use nitrate as a nitrogen source. Furthermore, we identified a specific growth condition that robustly decreases the abundance of pupylated proteins. This observation strongly suggests the presence of a yet-to-be-determined mechanism of control over the Pup-proteasome system in *M. tuberculosis* that is induced in nitrate.

INTRODUCTION

Mycobacterium tuberculosis (*M. tuberculosis*), the causative agent of the human disease tuberculosis, encodes a proteasome that is essential for its lethality in mice (1, 2). The central component of all proteasomes is a 28-subunit complex of four stacked rings known as the 20S core particle (20S CP). In *M. tuberculosis*, two identical outer rings, each composed of seven α-subunits (PrcA) serve as a gated entryway for protein substrates, and two identical inner rings, composed of a total of 14 β-subunits (PrcB), form the catalytic active sites of the protease (1, 3-5). While essential in eukaryotes and archaea, proteasomes are found only in a subset of bacteria primarily belonging to the *Actinomycetales* and *Nitrospirales* orders, and are not always essential for bacterial viability (6, 7).

In eukaryotes and bacteria, proteasomes carry out the regulated proteolysis of specific cellular substrates. Interest in the *M. tuberculosis* proteasome emerged after a screen for mutations that rendered this bacterial species sensitive to nitric oxide (NO), a host-derived molecule that is critical for controlling *M. tuberculosis* growth in mice (8), identified mutations in genes linked to *prcBA*. Over the years, it was determined that some proteasome substrates in *M. tuberculosis* are covalently modified with a small protein called Pup (prokaryotic ubiquitin-like protein) by a dedicated ligase, PafA (proteasome accessory factor A) (9-11). These pupylated proteins are recognized by a proteasomal activator, Mpa (mycobacterial proteasome ATPase, also known as ARC), which uses ATP hydrolysis to power the unfolding and delivery of proteins into 20S CPs for degradation (1, 12). Pup can also be removed from substrates by an enzyme called Dop (deamidase of Pup) (13, 14), as well as by PafA (15). Collectively, Dop, PafA, Pup, Mpa

and 20S CPs constitute the core "Pup-proteasome system" (PPS). At least sixty *M. tuberculosis* proteins are currently known to be pupylation substrates (9, 16, 17), while studies performed in other Pup-bearing bacteria, including *Mycobacterium smegmatis* (*M. smegmatis*), have identified hundreds of additional potential targets of pupylation (18-21). Of note, many pupylated proteins in *M. tuberculosis* are not degraded under routine culture conditions for reasons that remain unknown (16). This observation suggests pupylation may not immediately send proteins to the proteasome and could possibly serve a non-degradative regulatory role, as is observed in *Corynebacteria* (22).

In addition to being highly sensitive to NO *in vitro*, PPS mutants are highly attenuated for virulence in mouse infection models (2, 12, 23). The failure to degrade a single pupylated substrate, Log, is responsible for the NO hypersensitivity phenotype of a PPS (*mpa*) mutant. However, while genetic disruption of *log* completely restores NO resistance to an *mpa* strain *in vitro*, it does not fully rescue the virulence defect of this strain in mice (17). Therefore, there are likely to be other components of *M. tuberculosis* physiology whose regulation by the PPS is important for establishing lethal infections.

In addition to its central role in the post-translational regulation of various cellular pathways, an essential function of the eukaryotic proteasome is to maintain nutrient homeostasis by recycling amino acids (24, 25). In light of this observation, there has been interest in the question of whether or not the proteasome has a similar function in bacteria. Studies in *M. smegmatis* suggest that pupylation is required to maintain nitrogen homeostasis. Deletion of *pup* renders *M. smegmatis* more sensitive to nitrogen starvation (26), during which several enzymes involved in nitrogen metabolism are pupylated (21). In *M. tuberculosis*, amino acids serve as the primary nitrogen donors for most anabolic

processes (27, 28). Additionally, optimal *M. tuberculosis* growth, both *in vitro* and *in vivo*, requires the uptake of exogenous amino acids as a nitrogen source (29-32). It has therefore been hypothesized that the products of bulk proteolysis by the *M. tuberculosis* proteasome could be an important source of nitrogen under nutrient-limiting conditions. For this reason, we sought to determine if the *M. tuberculosis* proteasome contributed to nitrogen metabolism. Contrary to what was observed in *M. smegmatis*, we found that proteasomal degradation did not provide a survival advantage to *M. tuberculosis* during nitrogen starvation. However, we discovered that the proteasome was essential for the ability of *M. tuberculosis* to use nitrate as a nitrogen source. Through a genetic suppressor screen, we identified a putative PPS substrate whose inactivation rescued the ability of an *M. tuberculosis* PPS mutant to assimilate nitrogen from nitrate. Our data revealed an essential role for the PPS to facilitate the activity of nitrite reductase, possibly in two different ways, during growth in nitrate. Finally, we found that the abundance of the pupylome decreased when *M. tuberculosis* was grown in nitrate, the first condition known to alter proteasome substrate levels in *M. tuberculosis*.

RESULTS

The *M. tuberculosis* proteasome does not provide a survival advantage during nitrogen starvation *in vitro*. It has been previously reported that an *M. smegmatis pup* (also known as *prcS* in *M. smegmatis*) or *prcBA* mutant cannot survive as well as a wild type (WT) strain during several weeks of nitrogen starvation; however, the phenotypes of these mutants are almost fully complemented by *pup* alone, suggesting that proteasomal degradation itself may have a minor role in *M. smegmatis* nitrogen metabolism.

Nonetheless, it was proposed that the proteasome supported bacterial survival during nitrogen starvation by recycling amino acids (26). We therefore sought to test whether or not proteasomal degradation contributed to *M. tuberculosis* survival during nitrogen starvation. We incubated WT, Δ*mpa::hyg* ("*mpa*") and Δ*prcBA::hyg* ("*prcBA*") strains (see *SI Appendix*, Table S1) in Proskauer-Beck (PB) minimal medium lacking any nitrogen source and measured bacterial survival over time. In contrast to what is observed in *M. smegmatis*, we found that the WT strain had no survival advantage over the PPS mutant strains during three weeks of nitrogen starvation (Fig. 1A). Thus, amino acid recycling by the proteasome did not significantly contribute to nitrogen homeostasis in *M. tuberculosis* in our experiments. However, we cannot rule out a role for the proteasome in recycling amino acids under other conditions.

***M. tuberculosis* requires the PPS in order to use nitrate as a nitrogen source.** Following our observation that *M. tuberculosis* proteasome-defective strains did not have a survival disadvantage during nitrogen starvation, we next determined if the PPS was required for growth in a specific nitrogen source. *M. tuberculosis* can use both organic and inorganic sources of nitrogen, although asparagine and glutamate support growth most effectively *in vitro* (29). We compared the growth of WT and *mpa* strains in PB media supplemented with asparagine or glutamate, and found that the *mpa* mutant had a minor growth defect compared to the WT strain (Fig. 1B). When the same strains were provided the sub-optimal nitrogen sources arginine, ammonium, or nitrate, bacterial growth was predictably slower for both strains; remarkably, however, growth of the *mpa* mutant was almost completely abrogated in nitrate compared to the WT strain (Fig. 1C). A single copy

of *mpa* integrated on the chromosome restored growth of the *mpa* strain in nitrate (Fig. 1D).

To determine if the inability of an *mpa* mutant to use nitrate was specifically related to a failure to degrade pupylated proteins, we assessed the growth of a *pafA* mutant (*pafA*::MycoMarT7) and the *prcBA* strain. Both mutants were attenuated for growth similarly to an *mpa* mutant in PB-nitrate, demonstrating that both pupylation by PafA and proteolysis by 20S CPs were required for using nitrate as a sole nitrogen source (Fig. 1E).

M. tuberculosis uses a highly conserved pathway for nitrogen assimilation from nitrate (Fig. 1F). Once imported into the cell, nitrate is reduced to nitrite by the NarGHIJ nitrate reductase complex (33). Nitrite is then reduced to ammonium by the nitrite reductase complex NirBD (34). Finally, ammonium is incorporated into glutamate and glutamine, which comprise the major intracellular nitrogen pool (27). Notably, *M. tuberculosis* secretes into its extracellular space any nitrite that cannot be immediately reduced to ammonium (34).

We hypothesized that the inability of PPS mutants to productively grow in PB-nitrate was caused by a failure of one or more reactions within nitrate catabolism. Upon growing *M. tuberculosis* in PB-nitrate, we discovered that supernatants of *pafA*, *mpa*, and *prcBA* mutant cultures contained ten- to fifteen-fold higher concentrations of nitrite than those of a WT strain (Fig. 1G). This result suggested that these mutants, while capable of importing and reducing nitrate, were unable to reduce nitrite to ammonium, causing the secretion of excess nitrite. Further supporting this model, an *mpa* mutant strain was

159 capable of growing in PB-ammonium, which bypasses the requirement of nitrite reduction,
160 nearly as well as the WT strain (Fig. 1C).

161 In *M. tuberculosis*, the nitrite reductase complex is encoded by the *nirBD* (Rv0252-
162 Rv0253) operon. An *M. tuberculosis nirBD* mutant is unable to grow when nitrate is
163 provided as the single nitrogen source, implicating NirBD as the only nitrite reductase in
164 *M. tuberculosis* (34). Therefore, we hypothesized that degradation of one or more
165 pupylated proteins is required for the *in vivo* activity of NirBD.

166

167 **Suppressor mutations in *hrcA* or *nadD* restore growth of an *mpa* mutant in nitrate.**
168 Most of an *mpa* mutant culture ultimately dies upon extended incubation in PB-nitrate
169 (Fig. 1A), an observation that provided a powerful phenotype to screen for suppressor
170 mutations that might identify specific substrates of the PPS whose degradation is
171 necessary for NirBD activity. We previously generated a transposon mutant library of an
172 *M. tuberculosis mpa* strain, consisting of approximately 72,000 unique double-mutant
173 clones (17). To enrich for mutants with a suppressor phenotype, we incubated this library
174 in PB-nitrate for four to five weeks, until cultures were turbid. Surviving bacteria were
175 further expanded in rich media and subjected to a second round of incubation in PB-
176 nitrate. We isolated 16 clones from six independent pools and tested them individually for
177 growth in PB-nitrate. Interestingly, while all of the suppressor mutants grew more
178 productively than the parental *mpa* strain, no mutant grew as well as the WT strain (*SI*
179 *Appendix*, Fig. S1A).

180 To identify the suppressor mutations, we cloned DNA containing the transposon
181 insertion from each of the 16 isolates. We identified two strains with unique transposon

182 insertions in the coding region of *hrcA* (Rv2374c). The remaining suppressor strains
183 contained transposon insertions in different operons, with no obvious functional
184 connections. We therefore suspected that these strains had additional, spontaneous
185 mutations, possibly in *hrcA*. We PCR-amplified and sequenced the *hrcA* gene in the
186 remaining mutants and discovered that five more strains had point mutations in *hrcA*. We
187 next used whole-genome sequencing to identify mutations in the remaining nine
188 suppressor mutants; seven strains had mutations in either the promoter or coding region
189 of *nadD* (Rv2421c). Importantly, all of these suppressor mutations were the result of
190 independent events (see *SI Appendix*, Table S1).
191
192 **Expression of chaperonin genes promotes growth in nitrate.** Seven of the
193 suppressor strains had mutations in *hrcA*, which encodes a transcriptional repressor that
194 is conserved in many bacterial species as a regulator of molecular chaperones of the
195 Hsp60 family [reviewed in (35)]. In *M. tuberculosis*, HrcA directly represses four genes,
196 including three chaperonin-encoding genes *groES* (Rv3418c)*, groEL1* (Rv3417c), and
197 *groEL2* (Rv0440); and a fourth gene, Rv0991c, is uncharacterized (36) (Fig. 2A).
198 Chaperonins, which are represented in all domains of life, facilitate the folding of protein
199 substrates (37, 38). In bacteria, Hsp60-type chaperonins are composed of two stacked,
200 heptameric rings of Hsp60 (GroEL) subunits, forming a chamber in which proteins fold;
201 the chamber is capped by a heptamer of Hsp10 (GroES) subunits [reviewed in (39)]. *M.*
202 *tuberculosis* is unusual among prokaryotes by encoding two GroEL homologues, both of
203 which form complexes that are likely capped by GroES subunits (40). It was previously
204 shown that an *M. tuberculosis* strain with a deletion-disruption in *hrcA* exhibits high

205 expression of *groEL1, groEL2,* and *groES* genes, the products of which are detectable in
206 cell lysates by Coomassie brilliant blue staining of sodium dodecyl sulfate-polyacrylamide
207 (SDS-PAGE) gels (36). Using this method, we observed protein species corresponding
208 to GroEL1 or GroEL2 that were more abundant in an *mpa hrcA* double mutant (Δ*mpa::hyg*
209 *hrcA::*MycoMarT7) (Fig. 2B) and in an *hrcA* single mutant (Δ*hrcA*::*hyg*), as well as in the
210 other six *mpa hrcA* suppressor mutants (*SI Appendix*, Fig. S1B). We transformed an *mpa*
211 *hrcA* strain with an integrative plasmid encoding *hrcA* under the control of its native
212 promoter, creating strain MHD1344 (*SI Appendix*, Table S1). Complementation of the
213 *hrcA* mutation successfully restored GroEL to lower, WT levels (Fig. 2B), and reversed
214 the suppressor phenotypes, as observed by failed growth in PB-nitrate (Fig. 2C) and
215 excessive nitrite secretion (Fig. 2D). Collectively, these data support the hypothesis that
216 the expression of one or more genes of the HrcA regulon is required for nitrite reduction,
217 and that HrcA regulon expression is reduced in PPS mutants.

218 To assess gene expression in a PPS mutant, we performed a global transcriptional
219 analysis of WT and *mpa* strains grown in PB-nitrate by RNA sequencing (RNA-Seq) (see
220 Experimental Procedures). Because an *mpa* mutant cannot productively grow in this
221 media (Fig. 1C), we prepared RNA from cultures grown to early logarithmic phase [optical
222 density at 580 nm (OD_{580})=0.3]. RNA-Seq demonstrated that *groES* and *groEL2* were
223 repressed in an *mpa* mutant compared to the parental WT strain (Fig. 2E). The remaining
224 genes in the HrcA regulon, *groEL1* and Rv0991c, were also significantly repressed in an
225 *mpa* mutant, although by a factor of less than two-fold (Dataset S1). This analysis
226 suggested HrcA might be a PPS substrate.

227 To determine if the repression of the chaperonin genes leads to changes in protein
228 abundance, we measured global protein levels in WT and *mpa* strains grown in PB-nitrate
229 using tandem-mass-tag (TMT)-based quantitative mass spectrometry (MS) (see
230 Experimental Procedures). Quantitative MS demonstrated that both GroEL2 and GroES
231 were significantly less abundant in the *mpa* mutant compared to the WT strain; GroEL1
232 and Rv0991c levels were not significantly changed (Dataset S2).

233 *groES* and *groEL2* are essential (41), thus we were unable to disrupt these genes
234 to test their requirement for growth in PB-nitrate. However, previous work identified a
235 mutant with a transposon insertion in *groEL1* (1), and additionally, we deleted and
236 disrupted Rv0991c (ΔRv0991c::*hyg*) (*SI Appendix*, Table S1). Unlike a PPS mutant, the
237 *groEL1* and Rv0991c mutants grew well in PB-nitrate (*SI Appendix*, Fig. S2A). These data
238 suggest that the GroES-GroEL2 ("GroESL2") complex was needed for efficient nitrite
239 reduction.

240

241 **Chaperonin production promotes NirBD activity in *M. tuberculosis*.** In order to begin
242 to understand the association between chaperonins and nitrite reduction, we first checked
243 if NirB or NirD abundance varied in WT, *mpa* and *mpa hrcA M. tuberculosis* strains in our
244 MS data set (Dataset S2). While we observed a significant decrease in NirB abundance
245 in an *mpa* mutant compared to the WT strain, this phenotype was not reversed upon
246 disruption of *hrcA*; a similar trend was observed for NirD (*SI Appendix*, Fig. S2B). We thus
247 concluded that changes in NirBD abundance alone could not explain the differences in
248 nitrite reduction between the WT and *mpa* strains.

Bacterial chaperonins are required for folding many newly translated proteins, as well as for counteracting protein misfolding and aggregation under certain stress conditions (42-45). Consistent with this function of chaperonins, we always recovered less soluble protein from cell lysates of an *mpa* mutant than from the WT strain, a phenotype that was rescued by *hrcA* disruption (Fig. 2F). Based on these data, we hypothesized that chaperonins promote the activity of many *M. tuberculosis* proteins, including NirBD. To test this hypothesis, we measured NirBD activity in *M. tuberculosis* extracts. Bacterial extracts were supplemented with excess substrate (nitrite) and nicotinamide adenine dinucleotide (NAD), a cofactor that is required for NirBD activity (46). Compared to extracts made from the WT strain, nitrite reduction in *mpa* mutant extracts was at or below the limit of detection. Importantly, we observed a partial restoration of activity in *mpa hrcA* mutant extracts (Fig. 2G). This result suggested there was an intrinsic defect in NirBD activity in the *mpa* mutant that was restored by chaperonin overproduction. Notably, the incomplete rescue of nitrite reductase activity in an *mpa hrcA* strain might be explained by our observation that NirB levels were not restored by disruption of *hrcA* (*SI Appendix*, Fig. S2B).

HrcA can be pupylated *in vitro*. The observations that the HrcA regulon was repressed in an *mpa* mutant (Fig. 2E and Dataset S1) and that the disruption of *hrcA* rescued a growth defect of a PPS mutant (Fig. 2C) suggested that HrcA might be a proteasome substrate. To test this hypothesis, we first determined if HrcA could be pupylated *in vitro*. We purified *M. tuberculosis* HrcA with carboxyl-terminal FLAG and hexahistidine (His_6) tandem-affinity tags ($HrcA_{TAP}$) from *Escherichia coli* (*E. coli*). Following incubation of

272 $HrcA_{TAP}$ with purified His_6-Pup_{Glu} and PafA-His_6, which are sufficient to pupylate proteins,
273 we observed the appearance of a higher-molecular weight species corresponding to the
274 expected size of His_6-Pup~$HrcA_{TAP}$ (Fig. 3A, compare lanes 1 and 2). In *M. tuberculosis,*
275 proteins are usually pupylated at a specific lysine (16); we thus attempted to identify a
276 pupylation site on HrcA. We made several $HrcA_{TAP}$ variants, each with lysine-to-arginine
277 mutations in one or two of the six lysines in HrcA. Surprisingly, no single lysine was
278 essential for the *in vitro* pupylation of $HrcA_{TAP}$ (Fig. 3A, lanes 3 through 7). Meanwhile,
279 substitution of all six lysines abolished $HrcA_{TAP}$ pupylation (Fig. 3A, lane 8). Importantly,
280 because the epitope tag on $HrcA_{TAP}$ contained two non-native lysines, this experiment
281 demonstrated some substrate specificity for HrcA pupylation by PafA.

282 We sought to test if the pupylation of HrcA leads to its degradation *in vivo*.
283 However, we were unable to observe endogenous HrcA in *M. tuberculosis* under any
284 condition. We were unsuccessful in generating antibodies to detect HrcA in *M.*
285 *tuberculosis* lysates, and HrcA was barely detected by TMT-based quantitative MS
286 (Dataset S2). We also tried to use an epitope-tagged HrcA allele, but the tag abolished
287 its repressor function. Finally, we introduced an *hrcA* allele lacking all of its lysines into
288 an *hrcA* null mutant; however, this *hrcA* allele also completely lost its repressor activity.

289 Despite the technical limitations preventing us from observing pupylation or
290 degradation of HrcA *in vivo*, our observation that *mpa*, *pafA* or *prcBA* mutants could not
291 grow in nitrate (Fig. 1E) suggested that optimal chaperonin expression requires PPS-
292 dependent proteolysis. We therefore predicted that the HrcA regulon would be repressed
293 similarly in the *mpa* and *prcBA* mutants. We compared the abundance of GroEL2 in
294 lysates from WT, *mpa*, and *prcBA* strains grown in PB-nitrate. We observed a similarly

295 low abundance of GroEL2 in both the *mpa* and *prcBA* strains compared to the WT strain
296 (Fig. 3B). Collectively, the genetic evidence along with the pupylation assays suggest that
297 the degradation of HrcA is necessary for maintaining chaperonin gene expression in *M.*
298 *tuberculosis* grown in nitrate.
299
300 **Gain-of-function mutations in *nadD* rescue a defect in NAD availability in an *mpa***
301 **mutant.** We identified four different point mutations in *nadD* (nicotinate mononucleotide
302 adenylyltransferase) (*SI Appendix*, Table S1) that each rescued the growth of an *mpa*
303 mutant in PB-nitrate (Fig. 4A). NadD catalyzes a committed step in the biosynthesis of
304 NAD, a molecule that serves as an electron carrier in a wide variety of essential redox
305 reactions (47). Through ATP hydrolysis, NadD transfers adenosine monophosphate to
306 nicotinic acid mononucleotide (NaMN), generating nicotinic acid adenine dinucleotide
307 (NaAD), a direct precursor to NAD (48). In *M. tuberculosis*, NadD is constitutively required
308 for the production of NAD (49).
309 The four mutations we identified in *nadD* resulted in the amino acid substitutions
310 V62A, T105I, G131V, and G188A (V, valine; A, alanine; T, threonine; I, isoleucine; G,
311 glycine); two additional strains, recovered from independent mutant pools, also encoded
312 a $NadD_{V62A}$ allele (see *SI Appendix*, Table S1). Consistent with their ability to grow in PB-
313 nitrate, all four *mpa nadD* suppressor strains secreted low nitrite levels comparable to the
314 parental WT strain, demonstrating that NirBD activity was restored in these strains (Fig.
315 4B).
316 Because NadD is essential for the growth of *M. tuberculosis* (49), we predicted
317 that these *nadD* suppressor mutations resulted in a gain of function. To test this

hypothesis, we transformed a single copy of either WT *nadD* or *nadD*$_{V62A}$ into an *mpa* strain and assessed growth of these transformants in PB-nitrate. As expected, ectopic expression of *nadD*$_{V62A}$ partially rescued the growth of the *mpa* parental strain, while ectopic expression of WT *nadD* had an intermediate phenotype. Likewise, ectopic expression of *nadD*$_{V62A}$ had a dominant effect to reduce nitrite secretion, even in the presence of the endogenous, WT *nadD* (Fig. 4C). We also measured the levels of total oxidized and reduced NAD (NAD^+ and NADH, respectively) in *M. tuberculosis* lysates from our strains. Interestingly, we observed a nearly three-fold reduction in NAD abundance in an *mpa* mutant relative to the parental WT strain. Importantly, all four *nadD* mutations restored NAD abundance in an *mpa* mutant to levels equal to or greater than that of the WT strain (Fig. 4D). Thus, *nadD* gain-of-function mutations rescued a defect in NAD availability in the *mpa* strain.

NAD depletion could affect many redox-associated enzymes in *M. tuberculosis*; however, there exists a direct link between NAD and nitrate catabolism. NirBD catalyzes electron transfer from NADH to nitrite, producing ammonium and NAD^+ (50). This reaction also requires the presence of NAD^+ itself (46). Accordingly, the reduced levels of NAD in the *mpa* mutant could contribute to this strain's defect in NirBD activity.

We sought to understand the molecular basis by which amino acid substitutions in NadD result in increased production of NAD *in vivo*. We produced WT and variant (V62A, T105I, G131V, and G188A) NadD in *E. coli*, and purified these proteins to homogeneity. We first measured NadD protein stability using a thermal shift assay (see Experimental Procedures). Remarkably, three of the four NadD variants (T105I, G131V, G188A) displayed a more than 13ºC increase in melting temperature compared to WT NadD

(Table 1 and *SI Appendix*, Fig. S3A). We next measured the rate of ATP hydrolysis by WT and variant NadD upon incubation with NaMN. While NadD G131V and G188A hydrolyzed ATP at a higher rate, the remaining two NadD variants had less activity than the WT enzyme (Table 1).

We mapped the amino acid substitutions on the NadD crystal structure. T105I and G131V are located in the core of the NadD monomer (*SI Appendix*, Fig. S3B). This region is characterized by hydrophobic interactions between a central β-sheet and several α-helices (51); accordingly, such hydrophobic amino acid substitutions may stabilize NadD by increasing core packing, which might explain their increased thermal stability. In contrast, substitutions V62A and G188A lie at a subunit-to-subunit interface in the NadD tetramer (*SI Appendix*, Fig. S3B). NadD forms both dimers and tetramers *in vitro* (51); while the state of NadD assembly *in vivo* is unknown, it is possible that substitutions at the surface of NadD monomers influence the oligomeric state of NadD to affect its catalytic activity (either positively or negatively) in *M. tuberculosis*. While we cannot yet explain why two of the NadD mutant alleles show slower activity *in vitro*, our genetic data suggest NadD activity is higher *in vivo* for all four mutants.

We also found that the low NAD levels in an *mpa* mutant were also restored by disruption of *hrcA* (Fig. 4D). It is possible that either the HrcA regulon is needed to support NAD synthesis, or that in the absence of Mpa function, one or more NAD-consuming enzymes deplete the cellular stores of this cofactor.

Nitrogen sources affect steady state pupylome levels. Our results up to now suggest that the PPS degrades HrcA to allow for the expression of chaperonin genes in bacteria

364 growing in nitrate. However, we did not know whether these observations reflected the
365 specific degradation of HrcA, or a mass degradation of substrates by the proteasome. To
366 address this question, we grew *M. tuberculosis* in PB-Asn, which permits robust growth
367 of an *mpa* mutant (Fig. 1B), or in PB-nitrate and quantified the abundance of pupylated
368 proteins in bacterial lysates detectable by immunoblotting. We observed a nearly two-fold
369 decrease in pupylome abundance in bacteria grown in PB-nitrate compared to PB-Asn.
370 We also observed a decrease in the abundance of (unpupylated) inositol-3-phosphate
371 synthase (Ino1), a model PPS substrate (16), but not of PrcB (Fig. 5A). This result
372 suggested that there was an increase in the degradation of pupylated proteins, rather
373 than a decrease in pupylation, during growth in PB-nitrate. To further test this point, we
374 used a reporter protein, Pup-Zur-His_6, to specifically observe the degradation of a "pre-
375 pupylated" protein in *M. tuberculosis*. Zur (zinc uptake regulator, Rv2359) is an *M.*
376 *tuberculosis* protein that lacks lysines, and therefore cannot be pupylated *in vivo*. Pup is
377 translationally fused to Zur through a linear amide, rather than an isopeptide bond, and
378 cannot be depupylated; thus, the abundance of this reporter specifically assesses
379 proteolysis by the Mpa-proteasome (52). In WT *M. tuberculosis*, we observed a decrease
380 in Pup-Zur-His_6 abundance in bacteria grown in PB-nitrate compared to bacteria cultured
381 in PB-Asn. Meanwhile, in an *mpa* mutant, there was no difference in Pup-Zur-His_6 levels
382 upon growth in either medium, supporting a model whereby the Mpa-proteasome
383 degrades pupylated proteins during growth in nitrate (Fig. 5B).

384 Previous work has shown that total nitrogen starvation is associated with a
385 decrease in pupylated proteins in *M. smegmatis*. This phenomenon was attributed to a
386 greater abundance of 20S CPs upon nitrogen starvation, suggesting that *M. smegmatis*

regulates the production of the degradation machinery in response to nitrogen availability (26). However, we found that while the abundance of the pupylome, Ino1, and Pup-Zur-His_6 decreased during growth in PB-nitrate, the levels of Mpa, PrcA, and PrcB remained unchanged (Fig. 5B). Therefore, we propose that the regulation of proteasomal degradation in *M. tuberculosis* during growth in nitrate does not require significantly altering levels of the known proteolytic components.

DISCUSSION

In this work, we established that *M. tuberculosis* requires an intact PPS to assimilate nitrogen from nitrate. Specifically, the ability of *M. tuberculosis* to reduce nitrite depended on the expression of the Hsp60 chaperonin genes, including *groES* and *groEL2*. We found that HrcA, a repressor of the *groES and groEL1/2* genes, is most likely pupylated and degraded by the proteasome in order to allow for the production of the GroESL2 complex during growth in nitrate. Additionally, we found that NAD levels were reduced in the absence of a functional PPS, which could also contribute to the observed defect in nitrite reduction in PPS mutants. Lastly, we showed that the abundance of PPS substrates changed depending on the nitrogen source provided to *M. tuberculosis*.

While mouse models of *M. tuberculosis* infection have demonstrated a requirement for bacterial uptake of asparagine and aspartate as nitrogen sources (30, 31), the importance of nitrate as a nutrient during infection is less clear. An *M. tuberculosis narG* mutant, which is unable to reduce nitrate, is fully virulent in mice (53). However, unlike in humans, *M. tuberculosis* lesions in most inbred mouse lines are not hypoxic (53, 54); because nitrate import and reduction occur most abundantly under anaerobic conditions

410 (55-57), these infection models may not accurately reflect nitrate utilization during a
411 human infection.

412 Our results suggest that *M. tuberculosis* NirBD activity requires de-repression of
413 the HrcA regulon and support a model by which HrcA is degraded in a PPS-dependent
414 manner (Fig. 6). Studies of HrcA from other bacterial species have shown that this
415 repressor acts as a thermosensor: an increase in temperature induces the dissociation of
416 HrcA from DNA, presumably allowing for the expression of factors necessary to respond
417 to heat-induced protein misfolding (58, 59). We observed that the PPS alleviates HrcA
418 repression in the absence of heat shock, suggesting that there are other ways of inducing
419 the expression of the *hsp60* protein quality control genes in *M. tuberculosis*. Importantly,
420 it is unknown how many *M. tuberculosis* proteins depend on GroESL2 for folding. The
421 identification of other GroESL2 substrates could potentially uncover additional pathways
422 whose function depends on PPS-mediated control of chaperonin gene expression.
423 Importantly, these pathways may at least partially explain how defects in the PPS lead to
424 highly attenuated bacteria in animals.

425 According to the most well-characterized model of chaperonin activity in *E. coli*,
426 misfolded or unfolded proteins become encapsulated within a GroES-GroEL chamber, a
427 hydrophobic space in which substrates fold (37, 38). NirD has a mass of 12.5 kD, a size
428 that is within the range of most *E. coli* GroEL substrates (60); in contrast, the 90 kD NirB
429 subunit is too large to be fully encapsulated. Nonetheless, a mechanism of chaperonin-
430 mediated folding of large proteins without encapsulation has been described (61, 62), and
431 several high-molecular weight *E. coli* proteins have been identified as *in vivo* GroEL

substrates (60). Thus, it is possible that NirB and/or NirD are endogenous substrates of GroESL2 in *M. tuberculosis*.

While a failure of *M. tuberculosis* to maintain chaperonin levels is associated with a loss of NirBD function, we have also shown that an *mpa* mutant grown in nitrate lacks WT levels of NAD, which is required for NirBD activity. Proteomic analysis of WT and *mpa* strains did not identify alterations in the abundance of any enzymes within the NAD biosynthetic pathway that could explain the failure of an *mpa* mutant to maintain WT NAD levels (Dataset S2). It is possible that the NAD pool is exhausted by the accumulation of one or more PPS substrates that consume NAD. However, it is telling that in addition to compensatory mutations in *nadD*, *hrcA* disruption is sufficient to restore NAD levels in an *mpa* mutant. Taken together, these observations suggest that GroESL2 may also promote the folding or assembly of NadD or other enzymes in the NAD synthetic pathway. In turn, the gain-of-function mutations in *nadD* that were selected for in our suppressor screen may allow NadD to remain functional in spite of reduced chaperonin levels. Importantly, NadD is thought to be essential in most bacteria, and is of interest as a drug target in a potentially diverse set of pathogens, including *M. tuberculosis* (49, 63). Thus, the novel NadD variants that we describe here highlight the importance of NadD activity under stress conditions and strengthen the potential of NadD as an underappreciated drug target.

In a study using *M. smegmatis*, Gur and colleagues found that the pupylome is less abundant during nitrogen starvation, an observation that is similar to what we observed with *M. tuberculosis* grown in nitrate broth. It was proposed that altered levels of components of the PPS are responsible for this phenotype in *M. smegmatis* (26). In

455 contrast, we did not observe conspicuous changes in proteasome component abundance
456 in *M. tuberculosis* despite a dramatic change in substrate abundance, suggesting that
457 there are differences in the regulation of proteasomal activity between these bacterial
458 species. Instead of altering PPS component levels, it is conceivable that there are post-
459 translational modifications on the proteasome itself that alter its activity. For example, *M.*
460 *tuberculosis* kinases PknA and PknB can phosphorylate PrcA and PrcB (64); although
461 there is no indication that this activity occurs in a physiological setting, phosphorylation
462 could potentially affect the activity of 20S CPs. Additionally, there may be factors that
463 modulate the association of Mpa with the 20S CP, since attempts to observe a robust
464 Mpa-20S CP interaction *in vitro* have been unsuccessful (65).

465 In addition to identifying a novel role of the *M. tuberculosis* PPS in regulating
466 chaperonin and NAD levels during growth in nitrate, we found a specific condition during
467 which proteasomal degradation appears to be stimulated. Because the Hsp60 system is
468 undoubtedly required for the function of numerous proteins, it seems likely that other
469 environmental cues could activate proteasomal degradation to induce *hsp60* regulon
470 expression. Thus, the molecular mechanisms by which PPS function might be altered, as
471 well as other growth conditions that promote proteolysis, warrant further investigation.

472

473 **EXPERIMENTAL PROCEDURES**

474 **Bacterial strains, plasmids, primers, and culture conditions**. Bacterial strains,
475 plasmids, and primers used in this study are listed in *SI Appendix*, Table S1. Chemicals
476 used for making all buffers and bacterial media were purchased from ThermoFisher, Inc.
477 unless otherwise indicated. *M. tuberculosis* was grown in "7H9" [BD Difco Middlebrook

7H9 broth with 0.2% glycerol and supplemented with 0.5% bovine serum albumin (BSA), 0.2% dextrose, 0.085% sodium chloride, and 0.05% Tween-80]. For culturing *M. tuberculosis* in single nitrogen sources, a base of Proskauer-Beck (PB) minimal medium (66) with no nitrogen source ("PB-base") was prepared with 0.5% potassium phosphate monobasic, 0.06% magnesium sulfate heptahydrate, 1.5% glycerol, 0.25% magnesium citrate dibasic anhydrous, and 0.05% Tween-80. The following nitrogen sources were added to a final concentration of 10 mM: asparagine (PB-Asn), glutamate (PB-Glu), arginine (PB-Arg), sodium nitrate (PB-nitrate), or ammonium chloride (PB-ammonium); pH was adjusted to 6.4 after nitrogen addition. PB broths were autoclaved or filtered prior to use. *M. tuberculosis* was incubated at 37˚C for all experiments.

For solid media, *M. tuberculosis* was grown on "7H11" agar (BD Difco Middlebrook 7H11) containing 0.5% glycerol and supplemented with 10% final volume of BBL Middlebrook OADC Enrichment. For selection of *M. tuberculosis*, the following antibiotics were used as needed: kanamycin 50 µg/ml, hygromycin 50 µg/ml, and gentamicin 15 µg/ml.

E. coli was cultured in BD Difco Luria-Bertani (LB) broth or on LB-Agar. Media were supplemented with the following antibiotics as needed: kanamycin 100 µg/ml, hygromycin 150 µg/ml, and gentamicin 15 µg/ml.

For all experiments in which *M. tuberculosis* was cultured in PB broth, bacteria were first grown in 7H9 to an OD_{580} of 0.5 - 0.8, washed three times in PBS-T [phosphate buffered saline (Corning) with 0.05% Tween-80], and resuspended in the appropriate PB broth. For growth curves, bacteria were harvested by centrifugation at 500 $\times$ *g* for five minutes to remove large clumps of bacteria prior to dilution into fresh broth.

A detailed description of plasmid construction is provided in *SI Appendix,* Supplementary Experimental Procedures.

Protein purification, antibody production, and immunoblotting. Purification of PafA-His_6 and His_6-Pup_{Glu} was described previously (9, 15). HrcA was made with a C-terminal affinity tag consisting of FLAG and His_6 epitopes separated by a five-amino acid linker ("$HrcA_{TAP}$"). *M. smegmatis* PrcB was made with a C-terminal His_6 (smPrcB-His_6). $HrcA_{TAP,}$ smPrcB-His_6, and PrcA-His_6 were produced in *E. coli* strain ER2566 and purified by affinity chromatography using Ni-NTA agarose (Qiagen) according to the manufacturer's instructions (PrcA and PrcB were purified under urea denaturing conditions). To make rabbit polyclonal immune serum, approximately 200 µg PrcA-His_6 or smPrcB was used to immunize rabbits (Covance, Denver, PA). Purification of recombinant NadD is described in *SI Appendix*, Supplementary Experimental Procedures. Antibodies to *M. tuberculosis* DlaT were a gift from R. Bryk and C. Nathan.

Separation of proteins in *in vitro* assays and in *M. tuberculosis* lysates was performed using 10% sodium dodecyl sulfate-polyacrylamide (SDS-PAGE) gels, with the exception of the experiment shown in Fig. 5B, which used a 15% SDS-PAGE gel. Bio-Safe Coomassie Stain (Bio-Rad) was used to stain gels. For immunoblots, proteins were transferred from SDS-PAGE gels to nitrocellulose membranes (GE Amersham), and analyzed by immunoblotting as indicated. Detailed immunoblotting procedures are found in *SI Appendix*, Supplementary Experimental Procedures.

To quantify GroEL2 abundance in Fig. 3B, we used ImageJ (https://imagej.nih.gov) to measure the pixel density of GroEL2 and DlaT signals in immunoblot images. To

524 normalize each lane, the GroEL2 density was divided by the DlaT density. Quantification
525 of pupylome and Pup-Zur-His_6 abundances in Fig. 5 was performed in the same manner,
526 using the PrcB signal to normalize the pupylome or His signal for each lane. For the
527 fractionation experiment shown in Fig. 2F, total protein content in soluble and insoluble
528 lysate fractions was determined by separating samples on SDS-PAGE gels, staining gels
529 with Coomassie brilliant blue, and using ImageJ to measure pixel density in scanned
530 images.
531
532 **Preparation of *M. tuberculosis* extracts.** To generate protein extracts for gel separation
533 and immunoblotting, *M. tuberculosis* cultures were grown to an OD_{580} of 0.3. Equal
534 amounts of bacteria were harvested by centrifugation, resuspended in lysis buffer (50 mM
535 Tris, 150 mM sodium chloride, and 1 mM ethylenediaminetetraacetic acid (EDTA), pH
536 8.0). and transferred to a tube containing 250 µl of 0.1 mm zirconia beads (BioSpec
537 Products). Bacteria were lysed using a mechanical bead-beater (BioSpec Products).
538 Whole lysates were mixed with 4 × SDS sample buffer (250 mM Tris pH 6.8, 2% SDS,
539 20% 2-mercaptoethanol, 40% glycerol, 1% bromophenol blue) to a 1 × final concentration,
540 and samples were boiled for 5 minutes. For preparing lysates from *M. tuberculosis* grown
541 in 7H9, which contains BSA, an additional wash step with PBS-T was done prior to
542 resuspension of bacteria in lysis buffer.
543 For the fractionation experiment shown in Fig. 2F, bacteria were lysed as
544 described above; whole lysate was centrifuged at 16,000 × *g* for five minutes to pellet
545 insoluble material. Supernatants were mixed with 4 × SDS sample buffer, and pellets

546 were resuspended in 250 µl of fresh lysis buffer and mixed with 4 × SDS sample buffer;
547 each sample was boiled for 5 minutes.
548
549 **Sequencing of suppressor mutants.** *M. tuberculosis* chromosomal DNA was purified
550 as described previously (67). Transposon insertion sites were cloned from *M. tuberculosis*
551 genomic DNA, transformed into S17-λpir, and sequenced as previously described (1). For
552 strains MHD149, MHD1294, MHD1300, MHD1301, MHD1302, MHD1304, MHD1306,
553 MHD1307, MHD1308, and MHD1311, whole-genome sequencing was done by the
554 Genome Technology Center at NYU Langone Health using an Illumina Hi-Seq platform.
555 Reads were mapped to the H37Rv reference genome (NCBI) using BWA (http://bio-
556 bwa.sourceforge.net/) and SAMtools (http://samtools.sourceforge.net/). Identification of
557 nucleotide mutations was performed using HaplotypeCaller (Broad Institute).
558
559 **Quantification of nitrite reductase activity.** All experiments were performed using
560 cultures growing in PB-nitrate to an OD_{580} of 0.3. The concentration of nitrite in *M.*
561 *tuberculosis* culture supernatants was measured using the Griess assay (68) by mixing
562 supernatant 1:1 with Griess reagent (2.5% phosphoric acid, 0.5% sulfanilamide, 0.05%
563 N-(1-napthyl)-ethylenediamine), incubating for 10 minutes at 25˚C, and measuring
564 absorbance at 550 nm (A_{550}). A set of sodium nitrite solutions was used to make a
565 standard curve for A_{550} measurements.
566 Direct measurement of nitrite reductase activity in *M. tuberculosis* extracts was
567 performed as described previously, using NADH oxidation as a measure of NirBD activity
568 (46). To eliminate background oxidation by NADH dehydrogenase, a membrane-

associated complex, bacterial lysates were filtered and subjected to ultracentrifugation at 150,000 × *g* for 2 hours to remove insoluble material. Extracts were then normalized by total protein content after measuring the protein concentration using the Bio-Rad Protein Assay. NADH was measured in the reactions by A_{340}. Background NADH oxidation by extracts in the absence of sodium nitrite was measured and determined to be negligible.

Transcriptional analysis. To analyze gene expression, RNA was purified as previously described (69) from *M.* tuberculosis cultures grown in PB-nitrate to an OD_{580} of 0.3. Library preparation, sequencing by Illumina HiSeq, and analysis were performed by GENEWIZ, Inc. Sequence reads were mapped to the H37Rv genome using Bowtie2 (http://bowtie-bio.sourceforge.net/bowtie2/index.shtml). Unique gene hit counts were calculated using Subread (http://subread.sourceforge.net/), and differential gene expression analysis was performed using DeSeq2 (https://bioconductor.org/packages/release/bioc/html/DESeq2.html). To compare gene expression between strains, the Wald test was used to generate *p*-values and $\log_2$ fold changes. Genes with an adjusted *p*-value < 0.05 and absolute $\log_2$ fold change > 1 were called as differentially expressed genes for each comparison. Global gene expression analyses in WT and MHD149 strains is provided in Dataset S1. Raw sequencing data files are available in a PATRIC public workspace (https://patricbrc.org/workspace/public/shb360@patricbrc.org/shb2018).

Mass spectrometry: For analysis of protein content in *M. tuberculosis* strains, bacteria were grown in PB-nitrate to an OD_{580} of 0.3. Equal amounts of bacteria were harvested

by centrifugation, resuspended in freshly-prepared denaturing lysis buffer (100 mM Tris, 1 mM EDTA, 8M urea, pH 8.0), and lysed by bead beating. Whole lysates were centrifuged at 16,000 × g for 5 minutes to pellet the urea-insoluble material. Supernatants were centrifuged through a 0.22 µm Spin-X cellulose-acetate filter (Corning) and stored at -80ºC. Detailed methods for TMT-based quantitative MS are in *SI Appendix*, Supplementary Experimental Procedures. A comparison of global protein abundances between WT, MHD149, and MHD1297 is provided in Dataset S2. Raw peptide data is available in a PATRIC public workspace (https://patricbrc.org/workspace/public/shb360@patricbrc.org/shb2018).

***In vitro* pupylation of HrcA.** Pupylation assays were performed as described previously (10, 15). Briefly, reaction mixtures contained 1 µM His_6-Pup_{Glu}, 1 µM $HrcA_{TAP}$, and 0.5 µM PafA-His_6 at pH 8.0 in the presence of 5 mM ATP, 50 mM Tris, 20 mM magnesium chloride, 10% glycerol, 1 mM dithiothreitol, and 150 mM sodium chloride. Reactions were incubated overnight at 25˚C.

Quantification of NAD. Total NAD in *M. tuberculosis* lysates was quantified using the NAD/NADH Quantitation Kit (Sigma-Aldrich). Preparation of protein-free bacterial extracts and NAD quantification were performed according to the manufacturer's instructions.

NadD kinetics and stability assays. Thermal stability of NadD variants was measured using differential scanning fluorimetry (thermal shift assay). Differential scanning

615 fluorimetry was performed using a CFX96 Touch Real-Time PCR detection system and
616 the florescent dye SYPRO Orange stock concentration at a final concentration of 2 × in
617 96-well PCR plates. The initial fluorescence signal was measured after five minutes of
618 temperature equilibration at 25°C followed by measurements at every 1°C min^{-1} until
619 reaching 95°C. The wavelength of excitation and emission were 490 nm and 580 nm,
620 respectively. For each experiment, the protein was run alone and in the presence of 10
621 mM Mg-ATP. Experiments were carried out with at least three samples per condition;
622 results were expressed as mean values ± the standard error of the mean. Melting
623 temperatures were calculated using CFX Manager 3.1 software's d(RFU)/dT peak finder.
624 Reaction mixtures for the assay of nicotinic acid adenylyl transferase activity of
625 NadD contained 100 mM HEPES-NaOH, pH 7.4, 10 mM magnesium chloride, 1 mM
626 NaMN, 0.1 mM ATP (Sigma), 5 mU inorganic pyrophosphatase (Sigma) and 20 µg
627 purified NadD in a total volume of 0.1 ml. Reactions were performed in a clear, flat-
628 bottomed 96-well plate at room temperature. After incubation for 10 min., inorganic
629 phosphate was detected using the Malachite Green assay (70).
630
631 **Statistical significance**. With the exception of TMT-based proteomics and RNA-seq
632 analyses, all *p*-values were calculated using Welch's T-test.
633
634 **AUTHOR CONTRIBUTIONS**
635 S.H.B., J.B.J., A.D., K.V.K., B.U., and K.H.D. designed research; S.H.B., J.B.J., A.D.,
636 C.T.C., and J.S.R. performed research; S.H.B., K.V.K., and K.H.D. wrote the manuscript.
637

ACKNOWLEDGEMENTS

This work was supported by National Institutes of Health (NIH) grants R01 HL092774 and AI088075 awarded to K.H.D. S.H.B. and J.B.J. were supported by NIH grant T32 AT007180. S.H.B. also received support from the Jan T. Vilcek Endowed Fellowship Fund. K.V.K. was supported by NIH grant R03AI117361. We thank A. Osterman for providing the NadD expression construct. We thank C. Kenner, J. Li and R. Reed for assistance with NadD purifications. We thank S. Ehrt for the *prcBA* mutant and R. Copin for assistance in analysis of whole-genome sequencing data. We thank M. Samanovic, S. Zhang, A. Darwin, and members of the A. Darwin lab for helpful discussions.

REFERENCES

1. Darwin KH, Ehrt S, Gutierrez-Ramos JC, Weich N, & Nathan CF (2003) The proteasome of Mycobacterium tuberculosis is required for resistance to nitric oxide. *Science* 302(5652):1963-1966.
2. Gandotra S, Schnappinger D, Monteleone M, Hillen W, & Ehrt S (2007) In vivo gene silencing identifies the Mycobacterium tuberculosis proteasome as essential for the bacteria to persist in mice. *Nat Med* 13(12):1515-1520.
3. Lin G*, et al.* (2006) Mycobacterium tuberculosis prcBA genes encode a gated proteasome with broad oligopeptide specificity. *Mol Microbiol* 59(5):1405-1416.
4. Groll M*, et al.* (1997) Structure of 20S proteasome from yeast at 2.4 A resolution. *Nature* 386(6624):463-471.
5. Knipfer N & Shrader TE (1997) Inactivation of the 20S proteasome in Mycobacterium smegmatis. *Mol Microbiol* 25(2):375-383.
6. Becker SH & Darwin KH (2017) Bacterial Proteasomes: Mechanistic and Functional Insights. *Microbiol Mol Biol Rev* 81(1).
7. Lehmann G, Udasin RG, Livneh I, & Ciechanover A (2017) Identification of UBact, a ubiquitin-like protein, along with other homologous components of a conjugation system and the proteasome in different gram-negative bacteria. *Biochem Biophys Res Commun* 483(3):946-950.
8. MacMicking JD*, et al.* (1997) Identification of nitric oxide synthase as a protective locus against tuberculosis. *Proc Natl Acad Sci U S A* 94(10):5243-5248.
9. Pearce MJ, Mintseris J, Ferreyra J, Gygi SP, & Darwin KH (2008) Ubiquitin-like protein involved in the proteasome pathway of Mycobacterium tuberculosis. *Science* 322(5904):1104-1107.
10. Cerda-Maira FA*, et al.* (2011) Reconstitution of the Mycobacterium tuberculosis pupylation pathway in Escherichia coli. *EMBO Rep* 12(8):863-870.
11. Burns KE, Liu WT, Boshoff HI, Dorrestein PC, & Barry CE, 3rd (2009) Proteasomal protein degradation in Mycobacteria is dependent upon a prokaryotic ubiquitin-like protein. *J Biol Chem* 284(5):3069-3075.
12. Darwin KH, Lin G, Chen Z, Li H, & Nathan CF (2005) Characterization of a Mycobacterium tuberculosis proteasomal ATPase homologue. *Mol Microbiol* 55(2):561-571.
13. Burns KE*, et al.* (2010) "Depupylation" of prokaryotic ubiquitin-like protein from mycobacterial proteasome substrates. *Mol Cell* 39(5):821-827.
14. Imkamp F*, et al.* (2010) Deletion of dop in Mycobacterium smegmatis abolishes pupylation of protein substrates in vivo. *Mol Microbiol* 75(3):744-754.
15. Zhang S*, et al.* (2017) Mycobacterium tuberculosis Proteasome Accessory Factor A (PafA) Can Transfer Prokaryotic Ubiquitin-Like Protein (Pup) between Substrates. *MBio* 8(1).
16. Festa RA*, et al.* (2010) Prokaryotic ubiquitin-like protein (Pup) proteome of Mycobacterium tuberculosis [corrected]. *PLoS One* 5(1):e8589.
17. Samanovic MI*, et al.* (2015) Proteasomal control of cytokinin synthesis protects Mycobacterium tuberculosis against nitric oxide. *Mol Cell* 57(6):984-994.
18. Watrous J*, et al.* (2010) Expansion of the mycobacterial "PUPylome". *Mol Biosyst* 6(2):376-385.

19. Poulsen C*, et al.* (2010) Proteome-wide identification of mycobacterial pupylation targets. *Mol Syst Biol* 6:386.
20. Kuberl A*, et al.* (2014) Pupylated proteins in Corynebacterium glutamicum revealed by MudPIT analysis. *Proteomics* 14(12):1531-1542.
21. Fascellaro G*, et al.* (2016) Comprehensive Proteomic Analysis of Nitrogen-Starved Mycobacterium smegmatis Deltapup Reveals the Impact of Pupylation on Nitrogen Stress Response. *J Proteome Res* 15(8):2812-2825.
22. Kuberl A, Polen T, & Bott M (2016) The pupylation machinery is involved in iron homeostasis by targeting the iron storage protein ferritin. *Proc Natl Acad Sci U S A* 113(17):4806-4811.
23. Lamichhane G*, et al.* (2006) Deletion of a Mycobacterium tuberculosis proteasomal ATPase homologue gene produces a slow-growing strain that persists in host tissues. *J Infect Dis* 194(9):1233-1240.
24. Vabulas RM & Hartl FU (2005) Protein synthesis upon acute nutrient restriction relies on proteasome function. *Science* 310(5756):1960-1963.
25. Suraweera A, Munch C, Hanssum A, & Bertolotti A (2012) Failure of amino acid homeostasis causes cell death following proteasome inhibition. *Mol Cell* 48(2):242-253.
26. Elharar Y*, et al.* (2014) Survival of mycobacteria depends on proteasome-mediated amino acid recycling under nutrient limitation. *EMBO J* 33(16):1802-1814.
27. Viljoen AJ, Kirsten CJ, Baker B, van Helden PD, & Wiid IJ (2013) The role of glutamine oxoglutarate aminotransferase and glutamate dehydrogenase in nitrogen metabolism in Mycobacterium bovis BCG. *PLoS One* 8(12):e84452.
28. Gouzy A, Poquet Y, & Neyrolles O (2014) Nitrogen metabolism in Mycobacterium tuberculosis physiology and virulence. in *Nat Rev Microbiol*, pp 729-737.
29. Song H & Niederweis M (2012) Uptake of sulfate but not phosphate by Mycobacterium tuberculosis is slower than that for Mycobacterium smegmatis. *J Bacteriol* 194(5):956-964.
30. Gouzy A*, et al.* (2014) Mycobacterium tuberculosis exploits asparagine to assimilate nitrogen and resist acid stress during infection. *PLoS Pathog* 10(2):e1003928.
31. Gouzy A*, et al.* (2013) Mycobacterium tuberculosis nitrogen assimilation and host colonization require aspartate. *Nat Chem Biol* 9(11):674-676.
32. Rieck B*, et al.* (2017) PknG senses amino acid availability to control metabolism and virulence of Mycobacterium tuberculosis. *PLoS Pathog* 13(5):e1006399.
33. Stermann M, Sedlacek L, Maass S, & Bange FC (2004) A promoter mutation causes differential nitrate reductase activity of Mycobacterium tuberculosis and Mycobacterium bovis. *J Bacteriol* 186(9):2856-2861.
34. Malm S*, et al.* (2009) The roles of the nitrate reductase NarGHJI, the nitrite reductase NirBD and the response regulator GlnR in nitrate assimilation of Mycobacterium tuberculosis. *Microbiology* 155(Pt 4):1332-1339.
35. Narberhaus F (1999) Negative regulation of bacterial heat shock genes. *Mol Microbiol* 31(1):1-8.

36. Stewart GR, *et al.* (2002) Dissection of the heat-shock response in Mycobacterium tuberculosis using mutants and microarrays. *Microbiology* 148(Pt 10):3129-3138.
37. Martin J, Mayhew M, Langer T, & Hartl FU (1993) The reaction cycle of GroEL and GroES in chaperonin-assisted protein folding. *Nature* 366(6452):228-233.
38. Langer T, Pfeifer G, Martin J, Baumeister W, & Hartl FU (1992) Chaperonin-mediated protein folding: GroES binds to one end of the GroEL cylinder, which accommodates the protein substrate within its central cavity. *EMBO J* 11(13):4757-4765.
39. Hayer-Hartl M, Bracher A, & Hartl FU (2016) The GroEL-GroES Chaperonin Machine: A Nano-Cage for Protein Folding. *Trends Biochem Sci* 41(1):62-76.
40. Kong TH, Coates AR, Butcher PD, Hickman CJ, & Shinnick TM (1993) Mycobacterium tuberculosis expresses two chaperonin-60 homologs. *Proc Natl Acad Sci U S A* 90(7):2608-2612.
41. DeJesus MA, *et al.* (2017) Comprehensive Essentiality Analysis of the Mycobacterium tuberculosis Genome via Saturating Transposon Mutagenesis. *MBio* 8(1).
42. Susin MF, Baldini RL, Gueiros-Filho F, & Gomes SL (2006) GroES/GroEL and DnaK/DnaJ have distinct roles in stress responses and during cell cycle progression in Caulobacter crescentus. *J Bacteriol* 188(23):8044-8053.
43. Chapman E, *et al.* (2006) Global aggregation of newly translated proteins in an Escherichia coli strain deficient of the chaperonin GroEL. *Proc Natl Acad Sci U S A* 103(43):15800-15805.
44. Maisnier-Patin S, *et al.* (2005) Genomic buffering mitigates the effects of deleterious mutations in bacteria. *Nat Genet* 37(12):1376-1379.
45. Kerner MJ, *et al.* (2005) Proteome-wide analysis of chaperonin-dependent protein folding in Escherichia coli. *Cell* 122(2):209-220.
46. Coleman KJ, Cornish-Bowden A, & Cole JA (1978) Purification and properties of nitrite reductase from Escherichia coli K12. *Biochem J* 175(2):483-493.
47. Belenky P, Bogan KL, & Brenner C (2007) NAD+ metabolism in health and disease. *Trends Biochem Sci* 32(1):12-19.
48. Gerdes SY, *et al.* (2002) From genetic footprinting to antimicrobial drug targets: examples in cofactor biosynthetic pathways. *J Bacteriol* 184(16):4555-4572.
49. Rodionova IA, *et al.* (2014) Metabolic and bactericidal effects of targeted suppression of NadD and NadE enzymes in mycobacteria. *MBio* 5(1).
50. Kemp JD & Atkinson DE (1966) Nitrite reductase of Escherichia coli specific for reduced nicotinamide adenine dinucleotide. *J Bacteriol* 92(3):628-634.
51. Rodionova IA, *et al.* (2015) Mycobacterial nicotinate mononucleotide adenylyltransferase: structure, mechanism, and implications for drug discovery. *J Biol Chem* 290(12):7693-7706.
52. Burns KE, Pearce MJ, & Darwin KH (2010) Prokaryotic ubiquitin-like protein provides a two-part degron to Mycobacterium proteasome substrates. *J Bacteriol* 192(11):2933-2935.
53. Aly S, *et al.* (2006) Oxygen status of lung granulomas in Mycobacterium tuberculosis-infected mice. *J Pathol* 210(3):298-305.

54. Via LE, *et al.* (2008) Tuberculous granulomas are hypoxic in guinea pigs, rabbits, and nonhuman primates. *Infect Immun* 76(6):2333-2340.
55. Sohaskey CD & Wayne LG (2003) Role of narK2X and narGHJI in hypoxic upregulation of nitrate reduction by Mycobacterium tuberculosis. *J Bacteriol* 185(24):7247-7256.
56. Wayne LG & Hayes LG (1998) Nitrate reduction as a marker for hypoxic shiftdown of Mycobacterium tuberculosis. *Tuber Lung Dis* 79(2):127-132.
57. Akhtar S, Khan A, Sohaskey CD, Jagannath C, & Sarkar D (2013) Nitrite reductase NirBD is induced and plays an important role during in vitro dormancy of Mycobacterium tuberculosis. *J Bacteriol* 195(20):4592-4599.
58. Roncarati D, Danielli A, & Scarlato V (2014) The HrcA repressor is the thermosensor of the heat-shock regulatory circuit in the human pathogen Helicobacter pylori. *Mol Microbiol* 92(5):910-920.
59. Hitomi M, Nishimura H, Tsujimoto Y, Matsui H, & Watanabe K (2003) Identification of a helix-turn-helix motif of Bacillus thermoglucosidasius HrcA essential for binding to the CIRCE element and thermostability of the HrcA-CIRCE complex, indicating a role as a thermosensor. *J Bacteriol* 185(1):381-385.
60. Houry WA, Frishman D, Eckerskorn C, Lottspeich F, & Hartl FU (1999) Identification of in vivo substrates of the chaperonin GroEL. *Nature* 402(6758):147-154.
61. Chaudhuri TK, Farr GW, Fenton WA, Rospert S, & Horwich AL (2001) GroEL/GroES-mediated folding of a protein too large to be encapsulated. *Cell* 107(2):235-246.
62. Farr GW, *et al.* (2003) Folding with and without encapsulation by cis- and trans-only GroEL-GroES complexes. *EMBO J* 22(13):3220-3230.
63. Sorci L, *et al.* (2009) Targeting NAD biosynthesis in bacterial pathogens: Structure-based development of inhibitors of nicotinate mononucleotide adenylyltransferase NadD. *Chem Biol* 16(8):849-861.
64. Anandan T, *et al.* (2014) Phosphorylation regulates mycobacterial proteasome. *J Microbiol* 52(9):743-754.
65. Wu Y, *et al.* (2017) Mycobacterium tuberculosis proteasomal ATPase Mpa has a beta-grasp domain that hinders docking with the proteasome core protease. *Mol Microbiol* 105(2):227-241.
66. Atlas RM & Snyder JW (1995) *Handbook of media for clinical microbiology* (CRC Press, Boca Raton) pp v, 313 p.
67. van Soolingen D, Hermans PW, de Haas PE, Soll DR, & van Embden JD (1991) Occurrence and stability of insertion sequences in Mycobacterium tuberculosis complex strains: evaluation of an insertion sequence-dependent DNA polymorphism as a tool in the epidemiology of tuberculosis. *J Clin Microbiol* 29(11):2578-2586.
68. Stuehr DJ & Marletta MA (1985) Mammalian nitrate biosynthesis: mouse macrophages produce nitrite and nitrate in response to Escherichia coli lipopolysaccharide. *Proc Natl Acad Sci U S A* 82(22):7738-7742.
69. Festa RA, *et al.* (2011) A novel copper-responsive regulon in Mycobacterium tuberculosis. *Mol Microbiol* 79(1):133-148.

826 70. Sherwood AR, Paasch BC, Worby CA, & Gentry MS (2013) A malachite green-
827 based assay to assess glucan phosphatase activity. *Anal Biochem* 435(1):54-56.
828

829

FIGURE LEGENDS

Figure 1. The *M. tuberculosis* Pup-proteasome system (PPS) is required for growth in nitrate.

(A) The PPS does not promote survival of *M. tuberculosis* during complete nitrogen starvation. Survival of *M. tuberculosis* wild type (WT), *mpa* (MHD149), and *prcBA* strains was measured by number of colony-forming units (CFU) per ml of culture at the indicated time points. At week three, the fold change in CFU from input was determined to be statistically insignificant ($p > 0.05$) for *mpa* and *prcBA* strains compared to the WT strain. Experiment represents data from six replicate cutures. (B) The PPS is not essential for growth of *M. tuberculosis* in ideal nitrogen sources. Growth *of M. tuberculosis* strains in Proskauer-Beck (PB) minimal media supplemented with single nitrogen sources asparagine (PB-Asn) or glutamate (PB-Glu) was measured by optical density at 580 nm (OD_{580}). (C) An intact PPS is essential for *M. tuberculosis* growth when provided nitrate as the sole nitrogen source. *M. tuberculosis* strains were grown in PB supplemented with arginine (PB-Arg), nitrate (PB-nitrate), or ammonium (PB-ammonium). (D) Complementation of the *mpa* mutant growth defect in PB-nitrate. (E) Pupylation and proteasomal degradation are required for *M. tuberculosis* nitrate utilization, as assessed by the growth of *pafA* (MHD2), *mpa* (MHD5), and *prcBA* strains in PB-nitrate. (F) Schematic of the *M. tuberculosis* enzymes that catalyze reduction of nitrate to ammonium (33, 34). (G) PPS mutants (as in E) secrete excess nitrite into culture supernatants during growth in PB-nitrate. Experiments in (B) through (E) and (G) each contain data from three replicate cultures. ***, $p < 0.001$.

Figure 2. Disruption of *hrcA* increases chaperonin production and restores nitrite reductase activity to an *mpa* mutant.

(A) The *M. tuberculosis* HrcA regulon, illustrating operons repressed by HrcA. Positions of HrcA consensus binding sites are shown as gray squares (36). (B) A transposon mutation in *hrcA* results in the overproduction of chaperonins. Lysates from WT (MHD1350), *mpa* (MHD1352), *mpa hrcA* (MHD1347), and *mpa hrcA* complemented (MHD1344) strains were separated by SDS-PAGE, and proteins were stained with Coomassie brilliant blue. Molecular weight markers are indicated at left. Characteristic migration pattern of GroEL1 and GroEL2, which are similar in size, is indicated with an arrowhead. (C) Disruption of *hrcA* partially rescues the growth defect of an *mpa* mutant in PB-nitrate. (D) Disruption of *hrcA* returns bacterial nitrite secretion to WT levels in an *mpa* mutant during growth in PB-nitrate. <L.O.D., below the limit of detection. (E) The chaperonin genes are transcriptionally repressed in an *mpa* mutant (MHD149) compared to the WT parental strain. (F) The *mpa* mutant contains less soluble protein than WT or *mpa hrcA* (MHD1297) strains during growth in PB-nitrate. Additionally, the *mpa hrcA* strain contains less insoluble protein than WT or *mpa* strains. (G) An *mpa* mutant is defective in nitrite reduction, which is partially rescued by *hrcA* disruption. Nitrite reductase activity was measured in normalized protein extracts from bacteria grown in PB-nitrate. Extracts were supplemented with NADH, NAD^+, and nitrite, and nitrite reductase activity was assessed by measuring NADH oxidation over time (the nitrite reductase NirBD catalyzes electron transfer from NADH to nitrite to generate ammonium) (50). The difference in nitrite reductase activity between *mpa* and *mpa hrcA* lysates was determined to be statistically significant as indicated. Experiments in (C) through (G) each

876 contain data from three replicate cultures. Statistical significance is indicated as follows:
877 *, $p < 0.05$; **, $p < 0.01$; ***, $p < 0.001$. For all panels, "comp" indicated complementation
878 with *hrcA*.
879
880 **Figure 3. HrcA is a pupylated protein that is likely degraded by the *M. tuberculosis***
881 **proteasome.**
882 (A) Purified HrcA can be pupylated on any of its lysines by PafA. His_6-Pup_{Glu} and PafA-
883 His_6 were co-incubated with $HrcA_{TAP}$ WT or lysine-to-arginine (K>R) variants, and both
884 native and pupylated HrcA were detected by immunoblotting (IB) using an antibody that
885 recognizes an affinity tag on $HrcA_{TAP}$ (FLAG). Data are representative of three
886 independent experiments. (B) GroEL2 abundance is low in both *mpa* (MHD149) and
887 *prcBA* strains compared to the WT parental strain. Immunoblots for GroEL2 and
888 dihydrolipoamide acyltransferase (DlaT) were performed on the same membrane using
889 samples obtained from replicate PB-nitrate cultures. For each lane, GroEL2 was
890 normalized to DlaT, a protein that is not regulated by the PPS. The difference in
891 normalized GroEL2 abundance between strains is indicated at the bottom; for comparison
892 of WT and *mpa* strains, this difference had a *p*-value of 0.07; the difference in GroEL2
893 abundance between WT and *prcBA* strains had a *p*-value of < 0.01.
894
895 **Figure 4. Point mutations in *nadD* restore nitrate growth to an *mpa* mutant and**
896 **increase NAD abundance in bacteria.**
897 (A) Amino acid substitutions in NadD partially rescue growth of an *mpa* mutant in PB-
898 nitrate. Strains WT, MHD149, MHD1294, MHD1300, MHD1301, and MHD1311 are

represented. Note that strains MHD1294, MHD1300, MHD1301, and MHD1311 each have transposon insertions in unrelated genes (see *SI Appendix*, Table S1 for full genotypes). (B) *nadD* mutations restore nitrite secretion by the *mpa* strain to WT levels during growth in PB-nitrate. (C) Ectopic expression of WT *nadD* or $nadD_{V62A}$ partially rescues growth of an *mpa* mutant in PB-nitrate (left) and lowers nitrite secretion by the *mpa* mutant (right). Strains MHD1350, MHD1352, MHD1440, and MHD1456 are represented. (D) An *mpa* mutant contains less NAD than a WT strain, a defect that is rescued both by mutations in *nadD* and by disruption of *hrcA* (MHD1297). Total NAD [oxidized (NADH) and reduced (NAD^+) forms] was quantified in lysates of bacteria grown in PB-nitrate; statistical significance is indicated by comparison to the *mpa* single mutant. Experiments in (A) through (D) each contain data from three replicate cultures. **, $p < 0.01$; ***, $p < 0.001$.

Figure 5. Abundance of pupylated proteins depends on the nitrogen source.

(A) *M. tuberculosis* contains a lower abundance of pupylated proteins, and of a model PPS substrate, when grown in PB-nitrate compared to PB-Asn. Pupylated proteins were detected by immunoblot (IB) using a monoclonal antibody that recognizes *M. tuberculosis* Pup. The same immunoblot membranes were used to detect inositol-3-phosphate synthase (Ino1) and PrcB. The relative pupylome abundance between growth conditions (bottom) was normalized by PrcB abundance and was statistically significant ($p < 0.05$). (B) Pup-Zur-His_6 levels are reduced in WT *M. tuberculosis* grown in PB-nitrate compared to PB-Asn. The normalized Pup-Zur-His_6 intensity in the second lane relative to the first

lane is 0.62. PrcB and Mpa were detected on the same membrane, while PrcA was detected using a membrane separately prepared with the same lysates.

Figure 6. Model of PPS control over *M. tuberculosis* nitrate metabolism.

Left: HrcA, which represses the *M. tuberculosis* chaperonin genes including *groEL2*, is likely pupylated and degraded by the Mpa/20S CP proteasome to allow for the full expression of the chaperonins that promote the folding or assembly of the nitrite reductase NirBD. Middle: Failure of proteasomal degradation in *M. tuberculosis* leads to the repression of the chaperonin genes, preventing the formation of functional NirBD. Right: Disruption of *hrcA* restores NirBD activity in an *mpa* mutant through the full de-repression the chaperonin genes, while gain-of-function mutations in *nadD* increase the abundance of NAD to promote NirBD catalysis.

Table 1. Analysis of NadD variants.

Protein Sample	T_m (s.d.)[a], °C	Activity (s.d.), nmol min^{-1} mg^{-1}
NadD WT	54.4 (1.06)	1.09 (0.01)
NadD V62A	48.7 (0.94)	0.48 (0.015)
NadD T105I	68.0 (1.21)	0.11 (0.05)
NadD G131V	68.9 (0.82)	1.95 (0.005)
NadD G188A	67.7 (0.78)	2.34 (0.07)

[a]T_m, melting temperature; s.d., standard deviation.

Figure 1

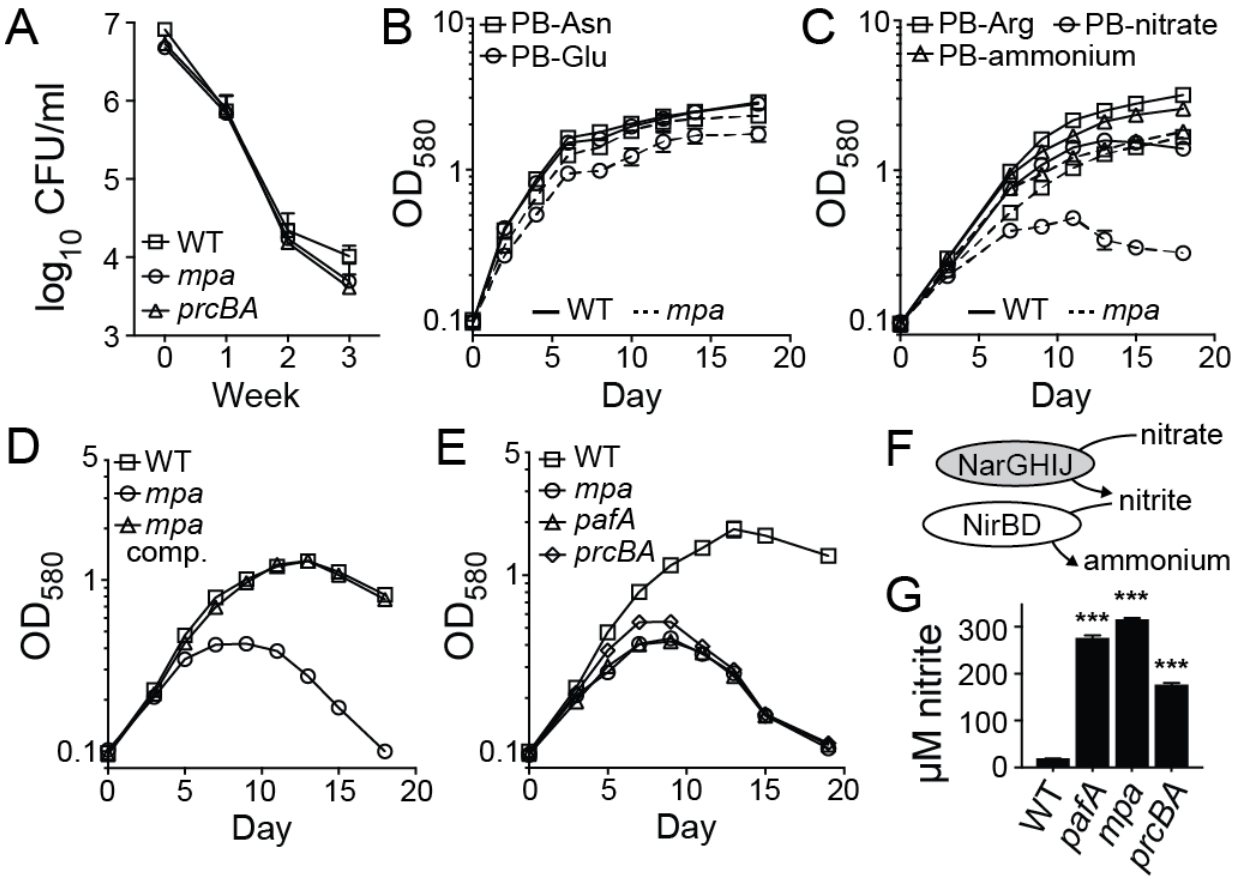

Figure 2

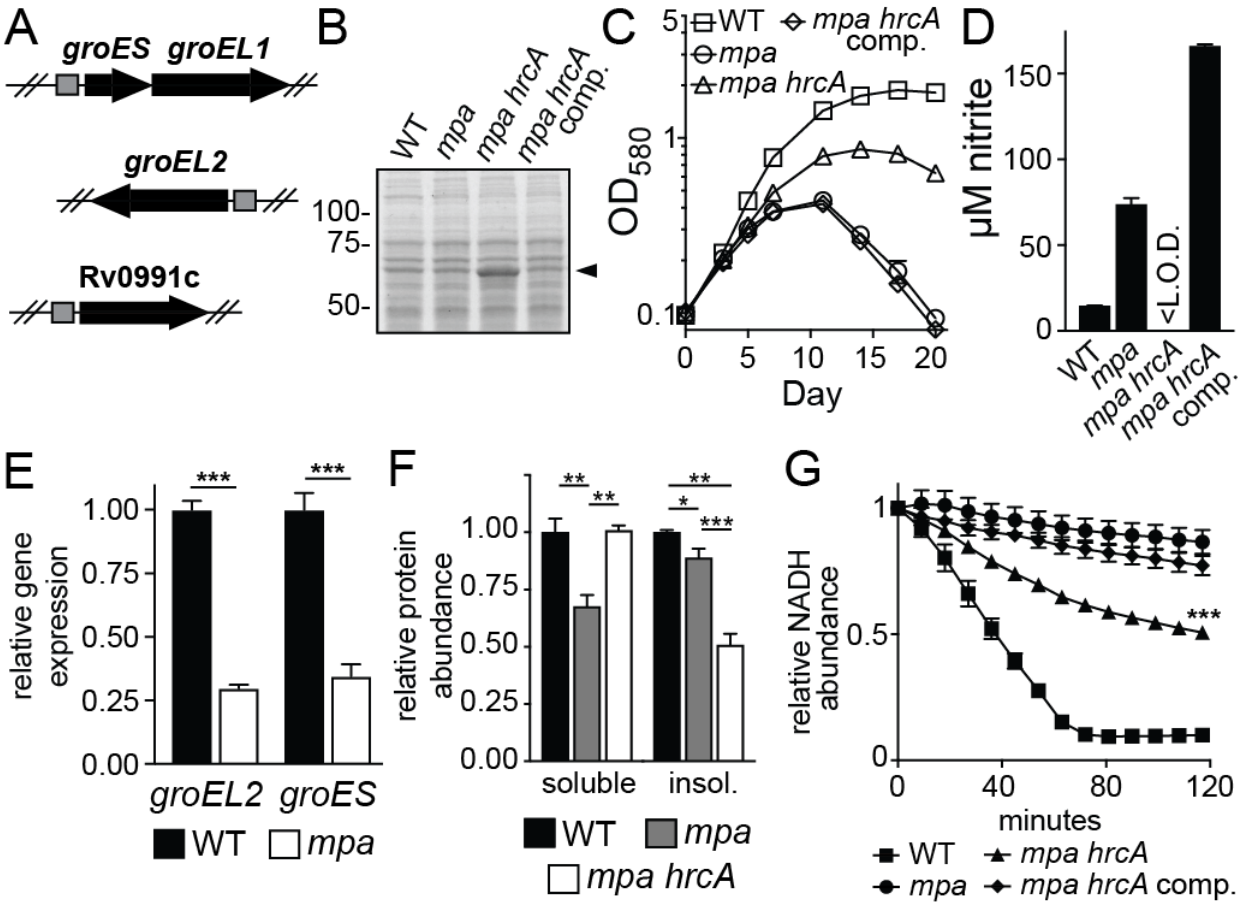

Figure 3

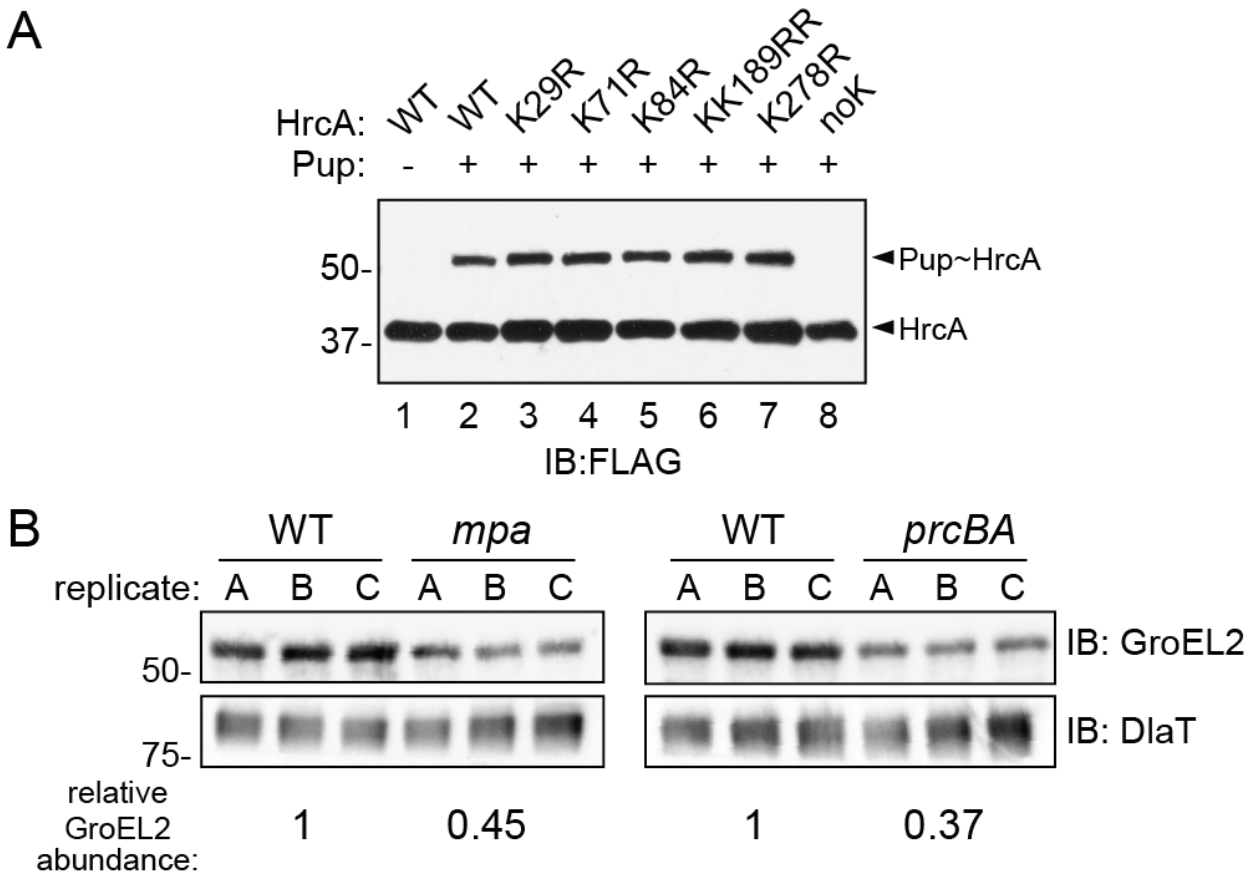

Figure 4

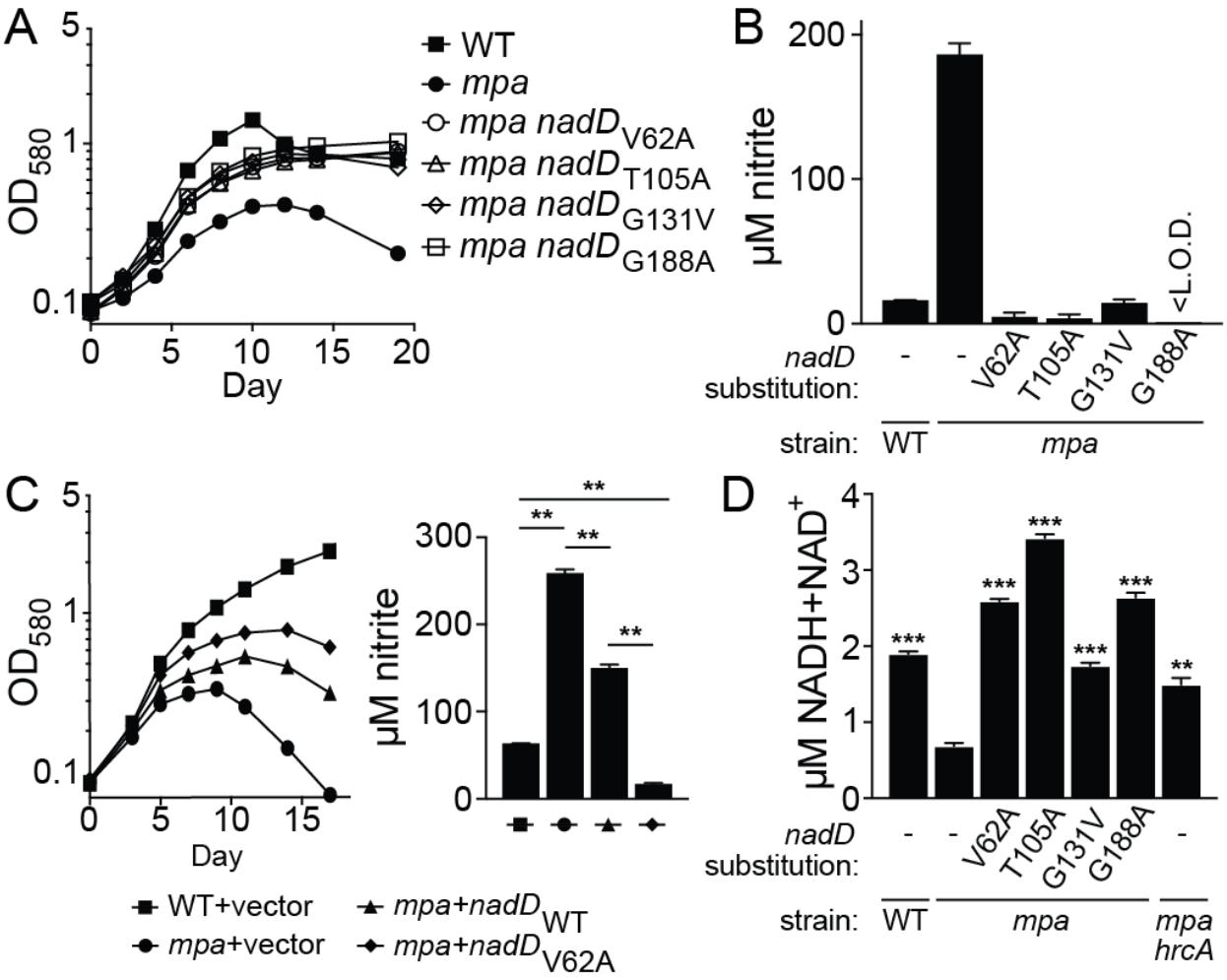

Figure 5

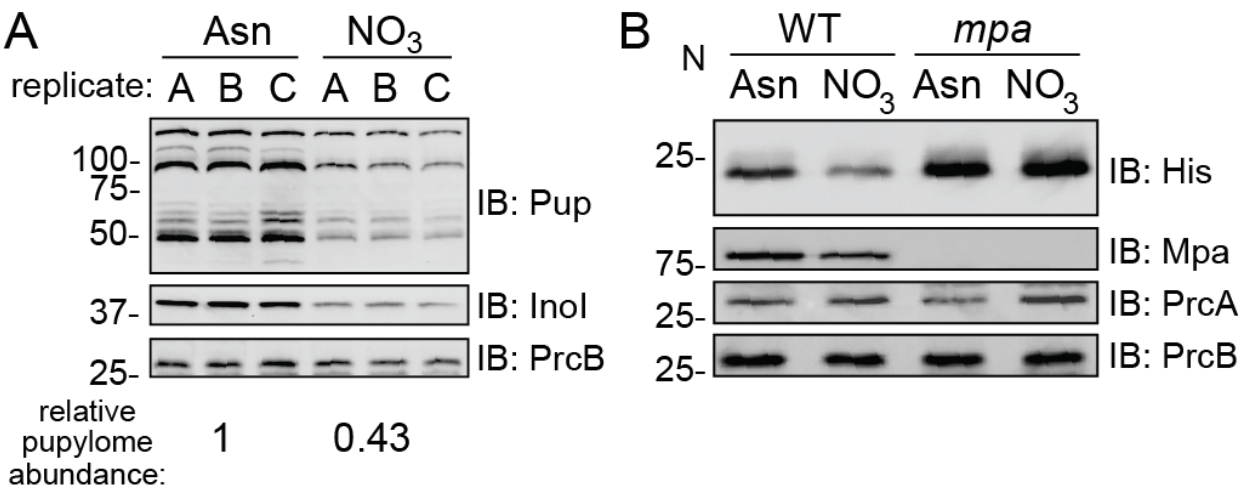

Figure 6

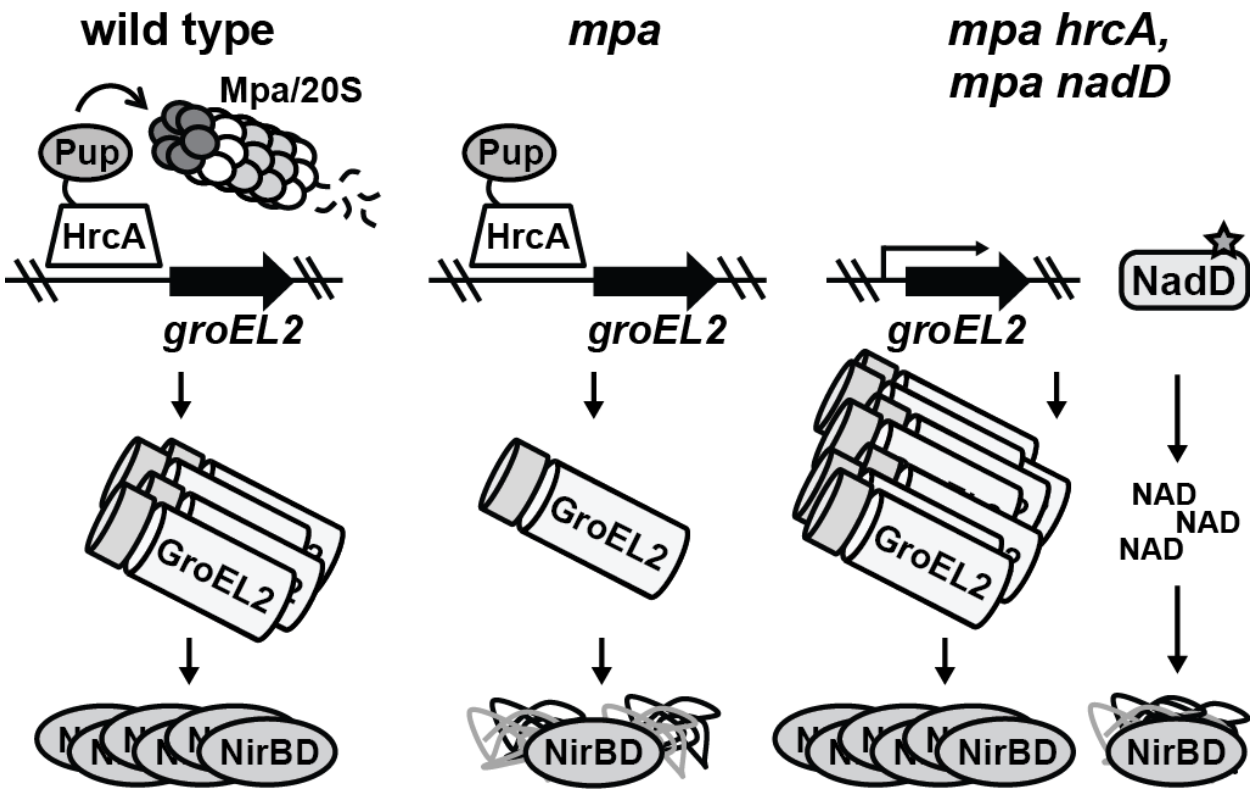

Supplementary Information for:

The *Mycobacterium tuberculosis* Pup-proteasome system regulates nitrate metabolism through an essential protein quality control system

Samuel H. Becker[1], Jordan B. Jastrab[1,2], Avantika Dhabaria[3], Catherine T. Chaton[4], Jeffrey S. Rush[4], Konstantin V. Korotkov[4], Beatrix Ueberheide[3], and K. Heran Darwin[1*]

[1]Department of Microbiology, New York University School of Medicine, 430 E. 29th Street, Suite 312, New York, NY 10016, USA

[2]Current address: Department of Medicine, Brigham and Women's Hospital, Boston, MA 02115, USA

[3]Proteomics Laboratory, Division of Advanced Research Technologies,

430 E. 29th Street, Suite 860, New York, NY 10016

New York University School of Medicine, New York, NY 10016, USA.

[4]Department of Molecular and Cellular Biochemistry, University of Kentucky,

741 S. Limestone Street, Lexington, KY 40536, USA

*Corresponding author: heran.darwin@med.nyu.edu

Classification: Biological Sciences: Microbiology

Keywords: *Mycobacterium tuberculosis*, proteasome, nitrate, chaperonins

This PDF file includes:

Table S1

Figures S1 to S3

Legends for Figures S1 to S3

Supplementary Experimental Procedures

References for SI Appendix

Other supplementary materials for this manuscript include the following:

Datasets S1 and S2

SUPPLEMENTARY TABLES AND FIGURES

TABLE S1. Strains, plasmids and primers used in this study.

M. tuberculosis strains

Strain	Relevant genotype or description	Source or reference
H37Rv	Wild type American Type Culture Collection (ATCC) #25618	ATCC
MHD5	Kan^R; *mpa*::MycoMarT7	(1)
MHD149	Hyg^R; Δ*mpa*::*hyg*	(2)
prcBA	Hyg^R; Δ*prcBA*::*hyg*	(3)
MHD18	Hyg^R; H37Rv, pMV306	(1)
MHD22	Hyg^R, Kan^R; MHD5, with pMV306	(1)
MHD23	Hyg^R, Kan^R; MHD5, with pMV306-*mpa*	(1)
MHD2	Kan^R; *pafA*::MycoMarT7	(1)
MHD1294	Kan^R,Hyg^R; *eccA1*::MycoMarT7, *nadD* codon 131 C>A (Gly131Val substitution)	This study
MHD1296	Kan^R,Hyg^R; Rv3256c::MycoMarT7, *hrcA* codon 56 T>C (Tyr56His substitution)	This study
MHD1297	Kan^R,Hyg^R; *hrcA*::MycoMarT7 inserted at codon 57	This study
MHD1298	Kan^R,Hyg^R; *ppsB*::MycoMarT7, frameshift mutation at *hrcA* codon 317	This study
MHD1299	Kan^R,Hyg^R; Rv0796::MycoMarT7, frameshift mutation at *hrcA* codon 138	This study
MHD1300	Kan^R,Hyg^R; *mazE3*::MycoMarT7, *nadD* codon 188 C>G (Gly188Ala substitution)	This study
MHD1301	Kan^R,Hyg^R; Rv3637::MycoMarT7, *nadD* codon 62 A>G (Val62Ala substitution)	This study
MHD1302	Kan^R,Hyg^R; PPE19::MycoMarT7, *nadD* codon 62 A>G (Val62Ala substitution)	This study
MHD1303	Kan^R,Hyg^R; *cobI*::MycoMarT7, duplication of *hrcA* codon 264 encoding a valine insertion	This study
MHD1304	Kan^R,Hyg^R; *cyp136*::MycoMarT7 inserted at codon 383	This study
MHD1305	Kan^R,Hyg^R; *hrcA*::MycoMarT7 inserted at codon 335	This study
MHD1306	Kan^R,Hyg^R; Rv0496::MycoMarT7, *nadD* codon 62 A>G (Val62Ala substitution)	This study
MHD1307	Kan^R,Hyg^R; *lppR*::MycoMarT7 inserted at codon 206	This study
MHD1308	Kan^R,Hyg^R; $nadD_P$::MycoMarT7 inserted 14 bases upstream of the *nadD* start codon	This study
MHD1309	Kan^R,Hyg^R; *cinA*::MycoMarT7, *hrcA* codon 32 G>A (Val32Met substitution)	This study
MHD1311	Kan^R,Hyg^R; *virS*::MycoMarT7, *nadD* codon 105 G>A (Thr105Ile substitution)	This study
MHD1350	Gm^R; MHD1, with pTT1B	This study
MHD1352	Gm^R, Hyg^R; MHD149, with pTT1B	This study

MHD1347	Gm^R, Hyg^R, Kan^R; MHD1297, with pTT1B	This study
MHD1344	Gm^R, Hyg^R, Kan^R; MHD1297, with pTT1B-*hrcA*	This study
MHD15	Kan^R; *groEL1*::MycoMarT7	(1)
MHD1384	Hyg^R; ΔRv0991c::*hyg*	This study
MHD1383	Hyg^R; Δ*hrcA*::*hyg*	This study
MHD1433	Gm^R, Hyg^R; MHD1383, with pTT1B	This study
MHD1434	Gm^R, Hyg^R; MHD1383, with pTT1B-*hrcA*	This study
MHD1456	Gm^R, Hyg^R; MHD149, with pTT1B-*nadD*	This study
MHD1440	Gm^R, Hyg^R; MHD149, with pTT1B-$nadD_{V62A}$	This study
MHD382	Hyg^R; MHD1, with pSYMP-*pup-zur-*his_6	(4)
MHD384	Hyg^R, Kan^R; MHD5, with pSYMP-*pup-zur-*his_6	(4)

E. coli strains

Strain	Relevant genotype or description	Source or reference
DH5a	*supE44* Δλ*acU169 (φ80 lacZΔM15) hsdR17 recA1 endA1 gyrA96 thi-1 relA1* (NalR)	Gibco
ER2566	F- λ- f*huA2* [*lon*] *ompT lacZ::T7 gene*I *gal sulA11* Δ(m*crC-mrr*)1*14::IS10 R(mcr-73*::miniTn*10*)2 *R*(*zgb-210*::Tn*10*)1 (tetS) *endA1* [*dcm*]	(5)
Rosetta (DE3)	F^- *ompT* $hsdS_B$(r_B^- m_B^-) *gal dcm* (DE3) pRARE (Cam^R)	EMD Millipore
S17-λpir	tpR strR *recA thi pro hsdR* RP4::2-Tc::Mu::Km Tn7 λpir lysogen	(6)

Plasmids

Plasmid	Description	Reference
pODC29-nadD-his_6	Amp^R; for purification of recombinant NadD with N-terminal His_6 tag	(7)
pODC29-$nadD_{V62A}$-his_6	Amp^R; for purification of recombinant $NadD_{V62A}$ with N-terminal His_6	This study
pODC29-$nadD_{T105I}$-his_6	Amp^R; for purification of recombinant $NadD_{T105I}$ with N-terminal His_6	This study
pODC29-$nadD_{G131V}$-his_6	Amp^R; for purification of recombinant $NadD_{G131V}$ with N-terminal His_6	This study
pODC29-$nadD_{G188A}$-his_6	Amp^R; for purification of recombinant $NadD_{G188A}$ with N-terminal His_6	This study
pET24b(+)	Kan^R; for inducible production of recombinant protein in *E. coli*	Novagen
pET24b(+)-*hrcA*-his_6	Kan^R; intermediate plasmid for construction of pET24b(+)-*hrcA*-TAP	This study
pET24b(+)-*hrcA*-TAP	Kan^R; for purification of recombinant HrcA with C-terminal FLAG-His_6	This study

pET24b(+)-*hrcA*$_{K29R}$ -TAP	Kan^R; for purification of recombinant HrcA$_{K29R}$ with C-terminal FLAG-His$_6$	This study
pET24b(+)-*hrcA*$_{K71R}$ -TAP	Kan^R; for purification of recombinant HrcA$_{K71R}$ with C-terminal FLAG-His$_6$	This study
pET24b(+)-*hrcA*$_{K84R}$-TAP	Kan^R; for purification of recombinant HrcA$_{K84R}$ with C-terminal FLAG-His$_6$	This study
pET24b(+)-*hrcA*$_{KK189RR}$-TAP	Kan^R; for purification of recombinant HrcA$_{KK189RR}$ with C-terminal FLAG-His$_6$	This study
pET24b(+)-*hrcA*$_{K278R}$-TAP	Kan^R; for purification of recombinant HrcA$_{K278R}$ with C-terminal FLAG-His$_6$	This study
pET24b(+)-*hrcA*$_{noK}$-TAP	Kan^R; for purification of recombinant HrcA lacking native lysines with C-terminal FLAG-His$_6$	This study
pET24b(+)-*prcA*-his$_6$	Kan^R; for purification of recombinant PrcA with C-terminal His$_6$	This study
pET24b(+)-*Msm-prcB*-his$_6$	Kan^R; for purification of recombinant PrcB with C-terminal His$_6$	This study
pYUB854	Hyg^R; for generation of *M. tuberculosis* mutants through allelic exchange	(8)
pYUB854-*hrcA*-KO2	Hyg^R; for generation of a deletion-disruption *hrcA* mutation in MHD1383	This study
pYUB854-Rv0991c-KO	Hyg^R; for generation of a deletion-disruption Rv0991c mutation in MHD1384	This study
pMV306	Hyg^R; for integration into the L5 *attB* site of the *M. tuberculosis* chromosome	(9)
pMV306-*mpa*	Hyg^R; *mpa* complementation plasmid	(1)
pTT1B	Gm^R; for integration into the Tweety *attP* site of the *M. tuberculosis* chromosome	(10)
pTT1B-*hrcA*	Gm^R; *hrcA* complementation plasmid	This study
pTT1B-*nadD*$_{WT}$	Gm^R; *nadD* complementation plasmid	This study
pTT1B-*nadD*$_{V62A}$	Gm^R; *nadD*$_{V62A}$ allele plasmid	This study
pSYMP-*pup-zur*-his$_6$	Hyg^R; for production of Pup-Zur-His$_6$ in *M. tuberculosis*	(4)

Primers

Primer name	**Primer sequence**
NdeI-hrcA-F	gatcCATATGggaagcgccgacgagcg
EcoRI-hrcA-R-nostop	ttaaGAATTCGGtcgagcacccaggacgtcgc
hrcA-K29R-F	CAACCCAGGAACCGATCGGCTCCAGATCCCTGGTGGAACGCCATAACCTG
hrcA-K29R-R	CAGGTTATGGCGTTCCACCAGGGATCTGGAGCCGATCGGTTCCTGGGTTG
hrcA-K71R-F	CGGACGCGTGCCCACGGAGAGGGGCTACCGCGAGTTCGTCGAC
hrcA-K71R-R	GTCGACGAACTCGCGGTAGCCCCTCTCCGTGGGCACGCGTCCG
hrcA-K84R-F	ttcgtcgaccggctcgaggacgtcAGAcccctatcgtcggccgagcgccgg
hrcA-K84R-R	ccggcgctcggccgacgatagggTCTgacgtcctcgagccggtcgacgaa

hrcA-KK189RR-F	atactcggccaggcgctggaaggcAGAAGActttcagcggcttcggtggcggtc
hrcA-KK189RR-R	gaccgccaccgaagccgctgaaagTCTTCTgccttccagcgcctggccgagtat
hrcA-K278R-F	CGGCTCAGCAGGAAGCCGGCAGGGTGACGGTTCGCATAGGTCATGAGAC
hrcA-K278R-R	GTCTCATGACCTATGCGAACCGTCACCCTGCCGGCTTCCTGCTGAGCCG
StuI-hrcAup-F	ttaaAGGCCTtcgtttgcgaacaagggcagtctg
XbaI-hrcAup-R	ttaaTCTAGAcatcgactgctcacctcacttcttac
HindIII-hrcAdown-F2	TTAAAAGCTTCGGCTGCTGGCGGCTCAGCA
BglII-hrcAdown-R	ttaaAGATCTcccgggcccgacctcgc
KpnI-Rv0991c-up-F2	ttaaGGTACCgcgttagtacttctgggcgtgacatcgttcacacgataac
XbaI-Rv0991c-up-R2	ttaaTCTAGAcacaagaacctccggaaatgtcactcggcgttagcactct
HindIII-Rv0991c-down-F	TTAAAAGCTTTGAGTTGAGAGGTTATCCACAAGGGG
BglII-Rv0991c-down-R	TTAAAGATCTGCCGGGATCATGCTCGTGGC
EcoRI-FLAG-NotI-F	gcgcGAATTCGgattacaaggatgacgacgataagGCGGCCGCatat
EcoRI-FLAG-NotI-R	atatGCGGCCGCcttatcgtcgtcatccttgtaatcCGAATTCgcgc
NdeI-prcA-F	ggttCATATGagttttccgtatttcatctcgcctgagca
HindIII-prcA-ns-R	ggccAAGCTTgcccgacgattcgccgtcaga
NcoI-nadD-F	tataCCATGGGCAtgcatgggcgtcgattgggagtca
PstI-nadD-R	tataCTGCAGTCATAGGCCATTCCCAGCGGCCAG
XbaI-hrcA-p-f	ttaaTCTAGAttgccttcccgcacccctttg
EcoRI-hrcA-R	ttaaGAATTCTCATCGAGCACCCAGGACGTC
XbaI-nadD-p-F	ggccTCTAGAacccagtcccgccccgtcgg
EcoRI-nadD-R	ggccGAATTCtcataggccattcccagcggcca
NdeIsmprcBF	GATCATATGacctggcgcgataatcagtcctttc
H3smprcBR	GAT-AAGCTTcgaatctcctcgcgcatcaatgc

FIGURE S1

A

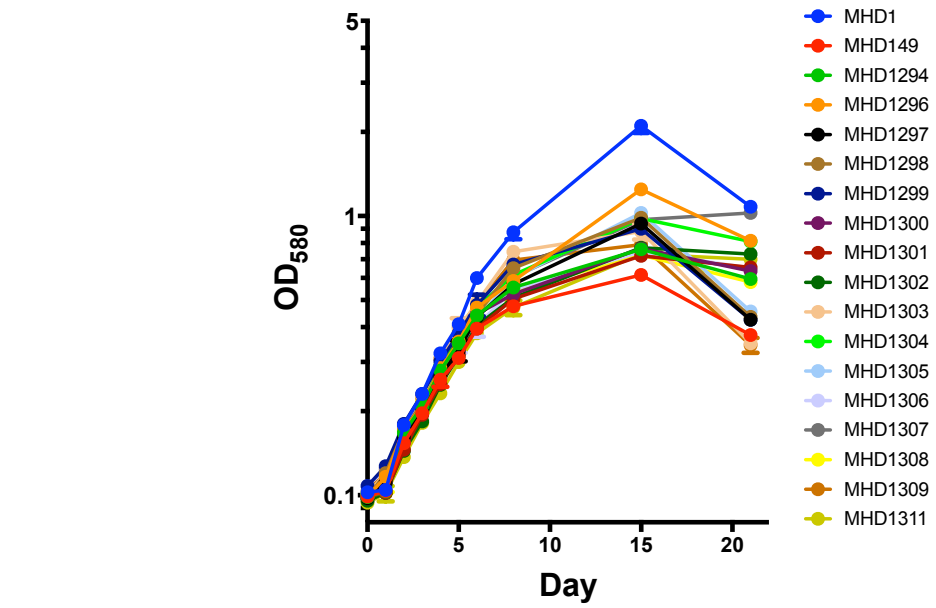

B

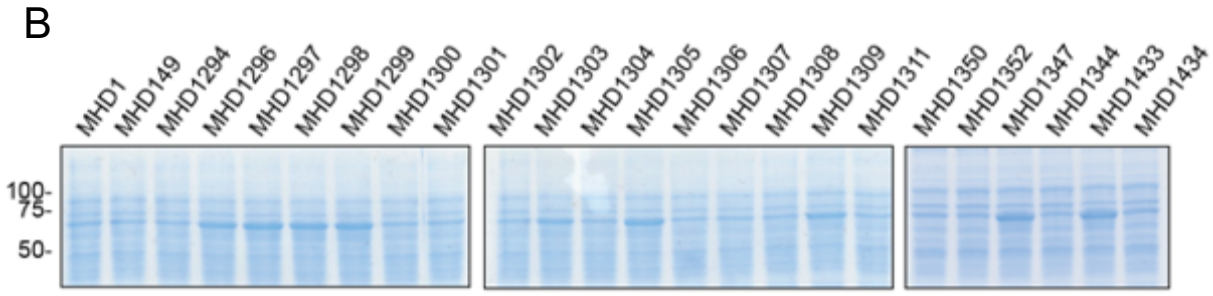

FIGURE S2

A

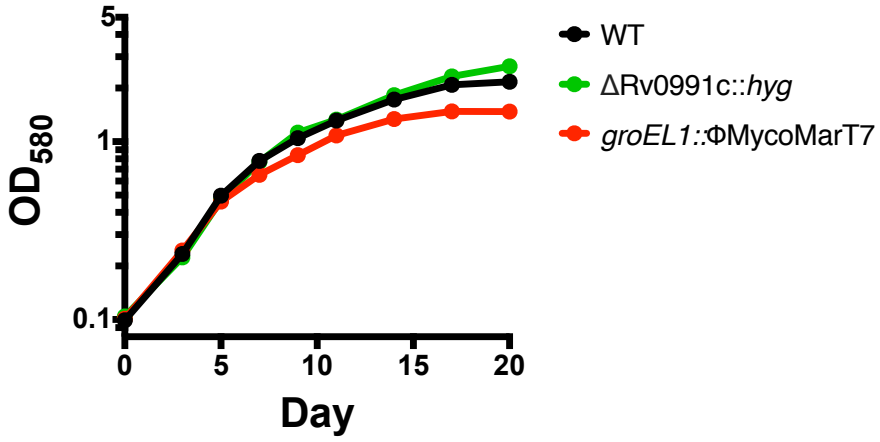

B

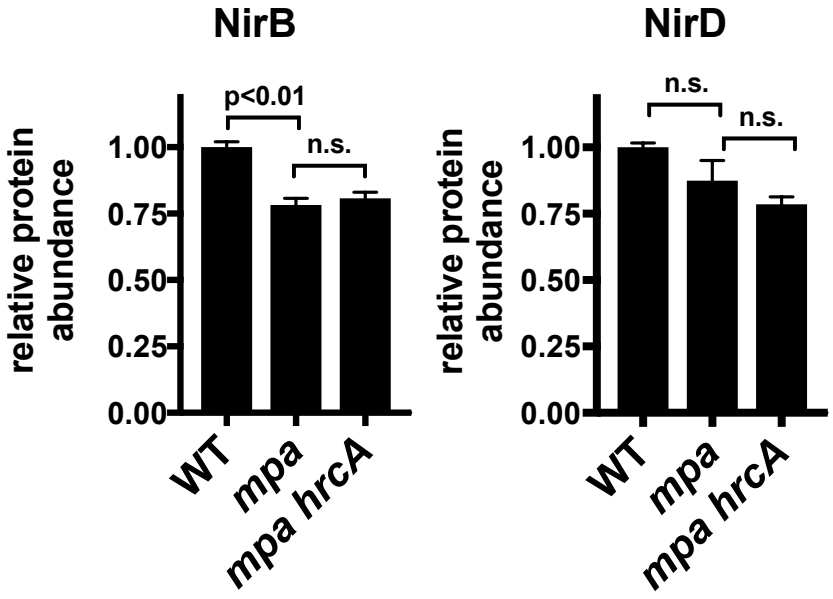

FIGURE S3

A

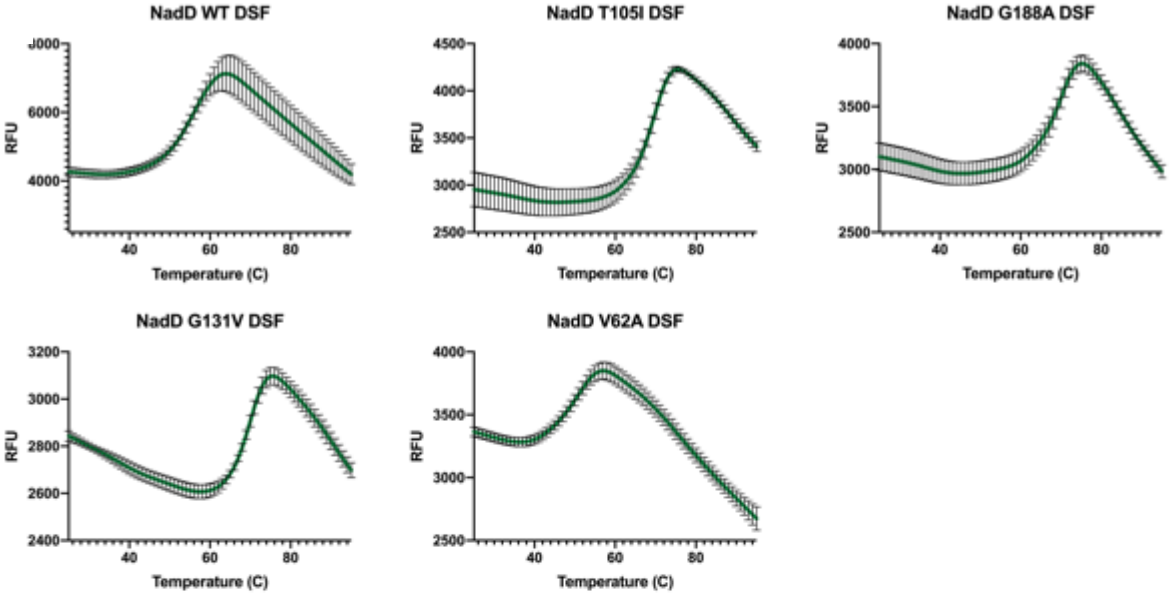

B

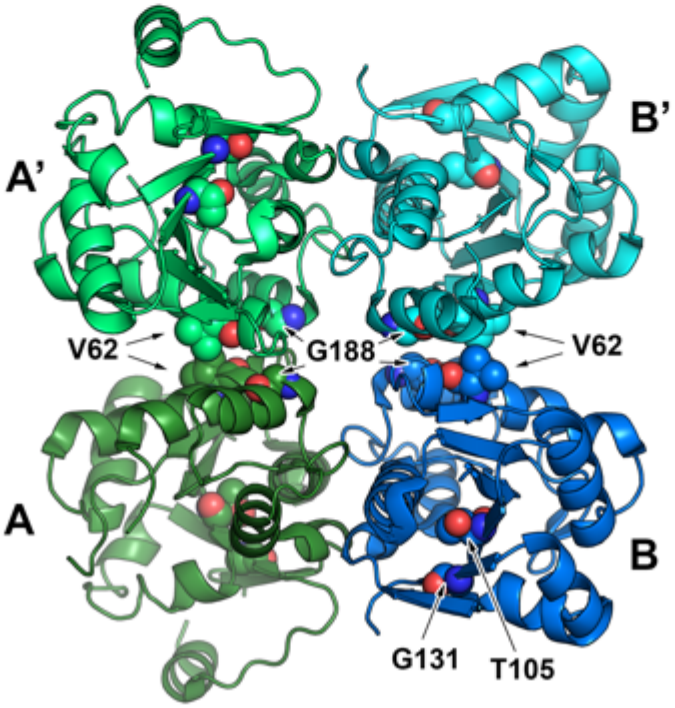

SUPPLEMENTARY FIGURE LEGENDS

Figure S1. (A) Growth of indicated strains (see Table S1) in PB-nitrate. (B) Assessment of GroEL1/GroEL2 levels in suppressor mutants. Lysates were prepared from indicated strains (see Table S1) grown in 7H9; proteins were separated by SDS-PAGE and stained with Coomassie brilliant blue.

Figure S2. (A) Strains with mutations in Rv0991c (MHD1384) or *groEL1* (MHD15) grow in PB-nitrate. (B) NirB is less abundant in *mpa* (MHD149) and *mpa hrcA* (MHD1297) strains compared to WT, and NirD abundance follows a similar trend although the difference did not reach statistical significance. Data in (B) are adapted from Dataset S1.

Figure S3. (A) Stability of purified WT NadD along with indicated NadD variants. Stability was determined by measuring protein melting temperature (T_m) using a thermal shift assay (see Experimental Procedures in the main text). T_m values are summarized in Table 1. (B) Location of NadD mutations in the structure of *M. tuberculosis* NadD. A tetrameric structure of NadD (PDB: 4X0E) (7) is shown in cartoon representation. Mutated residues are shown as spheres. Chains A and B (which are present in the asymmetric unit) form a tetramer with the crystallographic symmetry chains A' and B'.

SUPPLEMENTARY EXPERIMENTAL PROCEDURES

Primers and plasmid construction. Table S1 contains a list of all primers and plasmids used in this study. Primers used for PCR amplification were purchased from Life Technologies. DNA was PCR-amplified using polymerases Phusion (New England Biolabs; NEB), Pfu (Agilent), or Taq (Qiagen) according to the manufacturers' instructions. Plasmids encoding single- or double- lysine-to-arginine $HrcA_{TAP}$ variants were constructed using overlap extension PCR (11). Amplified DNA was purified using the QIAquick Gel Extraction Kit (Qiagen). Restriction enzymes and T4 DNA ligase used for cloning were purchased from NEB, and cloning was performed in *E. coli* strain DH5α. Plasmids were purified from *E. coli* using the QIAprep Spin Miniprep Kit, and DNA was sequenced by GENEWIZ, Inc. to ensure the veracity of the cloned sequence. To generate pET24b(+)-*hrcA*-TAP by inserting the FLAG sequence directly upstream of His_6, primers EcoRI-FLAG-NotI-F and EcoRI-FLAG-NotI-R were annealed and cloned into pET24b(+)-*hrcA*-his_6. To construct pET24b(+)-$hrcA_{noK}$-TAP, a plasmid harboring an *hrcA* allele with mutations in all six native lysine codons ($hrcA_{noK}$) was constructed using gene synthesis (GENEWIZ, Inc.); $hrcA_{noK}$ was subcloned into pET24b(+)-*hrcA*-TAP. To generate mutant variants of NadD, *nadD* mutant alleles were PCR-amplified from respective *M. tuberculosis* strains and cloned into the previously described construct for *M. tuberculosis* NadD expression in *E. coli* (7) (Table S1).

Deletion-disruption mutations in *hrcA* and Rv0991c (strains MHD1383 and MHD1384, respectively) were generated using allelic exchange plasmids to replace the respective genes with a hygromycin resistance cassette, as described in detail previously

(8). For allelic exchange using pYUB854-*hrcA*-KO2, the last 77 codons of *hrcA* were maintained in order to preserve the promoter of the downstream gene, *dnaJ2* (Rv2373c). Successful allelic exchange in mutant strains was confirmed by PCR-amplifying and sequencing the deletion-disruption site from the chromosome.

Plasmids were transformed into *M. tuberculosis* by electroporation as previously described (12). Single-colony transformants were isolated on 7H11 with antibiotic selection.

Purification of recombinant NadD. To obtain NadD WT and mutant variants, Rosetta (DE3) *E. coli* competent cells were transformed with the relevant plasmids and grown to an OD_{600} of 1.5-1.7 at 37 °C with shaking. 400 μM Isopropyl β-D-thiogalactopyranoside (IPTG) was added and the cells were allowed to express for 4.5 hours at 37 °C. Because all four mutants displayed some level of cytotoxicity, the cells were grown to a higher density and allowed to express for a shorter time than is typical to minimize cell death while still providing acceptable protein yields. Pellets were obtained by centrifugation and cells were lysed with ThermoFisher's bacterial protein extraction reagent (B-PER), lysozyme, and DNase at 25 °C for 1 hour. Protein was purified from filtered lysate by passage over a Ni-affinity column containing HisPur Superflow agarose (Thermo Fisher Scientific). Under these conditions, NadD co-purifies in a complex with NAD phosphate ($NADP^+$). After washing with 20 mM Tris-HCl at pH 7.5, 300 mM sodium chloride, 10 mM imidazole, $NADP^+$ was dissociated from NadD by three successive washes with buffer containing 20 mM Mg-ATP. Each wash was allowed a 20 min incubation. Mg-ATP was then removed by passage of three buffer washes with 15 min incubations before final

elution using 20 mM Tris-HCl at pH 7.5, 300 mM sodium chloride, 250 mM imidazole. After overnight dialysis at 4°C to remove the imidazole, the protein was then further purified on a Superdex 200 10/300 Increase (GE Healthcare). The collected protein was then concentrated to 1 mg/ml using an Amicon Ultra-50 10 kD cutoff centrifugal filter unit before being flash frozen in liquid nitrogen.

Detailed immunoblotting procedures. Antibodies used in this study: FLAG M2 monoclonal antibody (Sigma-Aldrich) was used according to the manufacturer's instructions; for Pup-Zur-His_6 we used PentaHis Antibody (Qiagen); for GroEL2 immunoblots we used the NR-13655 monoclonal antibody to *M. tuberculosis* GroEL2 (BEI Resources) at a concentration of 1:1000 in 3% BSA; for Pup, we used an *M. tuberculosis* Pup-specific monoclonal antibody (13) at 1:1000 in 3% BSA; for DlaT immunoblots, DlaT antiserum (14) was used at 1:5,000 in 3% BSA; polyclonal rabbit antisera to InoI (15), Mpa (16), PrcB and PrcA were used at a 1:1000 dilution in 3% BSA. Secondary antibodies HRP-conjugated goat anti-rabbit IgG F(ab')2 and HRP-conjugated anti-mouse IgG(H+L) were purchased from Thermo Fisher Scientific. All primary and secondary antibodies were made or diluted in 25 mM Tris-Cl/125 mM NaCl/0.05% Tween 20 buffer (TBST). Immunoblots were developed using SuperSignal West Pico PLUS chemiluminescent substrate (Thermo Fisher Scientific) and imaged using a Bio-Rad ChemiDoc system.

Detailed mass spectrometry procedures. Following preparation of lysates from *M. tuberculosis* as described in the main text, 150 µg of each protein lysate were reduced using dithiothreitol (5 µl of 0.2 M) for 1 h at 55 °C. The reduced cysteines were

subsequently alkylated with iodoacetamide (5 µl of 0.5 M) for 45 min in the dark at room temperature. Next, 20 mM HEPES (pH 8.0) was added to dilute the urea concentration to 2 M. Protein lysates were digested with Trypsin (Promega) at a 100:1 (protein:enzyme) ratio overnight at room temperature. The pH of the digested protein lysates was lowered to pH < 3 using trifluoroacetic acid (TFA). The digested lysates were desalted using C18 solid-phase extraction (Sep-Pak, Waters). 40% acetonitrile (ACN) in 0.5% acetic acid followed by 80% ACN in 0.5% acetic acid was used to elute the desalted peptides. The peptide eluate was concentrated in a SpeedVac and stored at -80°C.

For tandem-mass-tag (TMT) labeling, the dried peptide mixture was re-suspended in 100 mM TEAB (pH 8.5) using a volume of 100 µl, and each sample was labeled with TMT reagent according to the manufacturer's protocol (Thermo Fisher Scientific). In brief, each TMT reagent vial (0.8 mg) was dissolved in 41 µl of anhydrous ethanol and was added to each sample. The reaction was allowed to proceed for 60 min at room temperature and then quenched using 8 µl of 5% weight/volume hydroxylamine. The samples were combined at a 1:1 ratio and the pooled sample was subsequently desalted using SCX and SAX solid-phase extraction columns (Strata, Phenomenex) as described (17).

A 500 µg aliquot of pooled sample was fractionated using basic pH reverse-phase HPLC as previously described (18). Briefly, the sample was loaded onto a 4.6 mm × 250 mm Xbridge C18 column (Waters, 3.5 µm bead size) using an Agilent 1260 Infinity Bio-inert HPLC and separated over a 70 min linear gradient from 10 to 50% Buffer B in Buffer A at a flow rate of 0.5 ml/min (Buffer A = 10 mM ammonium formate, pH 10.0; Buffer B = 90% ACN, 10 mM ammonium formate, pH 10.0). A total of 40 fractions were

collected throughout the gradient. The early, middle and late eluting fractions were concatenated and combined into 10 final fractions. The combined fractions were concentrated in the SpeedVac and stored at -80°C until further analysis.

For analysis by liquid chromatography with tandem mass spectrometry (LC-MS/MS), an aliquot of each sample was loaded onto a trap column (Acclaim® PepMap 100 pre-column, 75 µm × 2 cm, C18, 3 µm, 100 Å, Thermo Scientific) connected to an analytical column (EASY-Spray column, 50 m × 75 µm ID, PepMap RSLC C18, 2 µm, 100 Å, Thermo Scientific) using the autosampler of an Easy nLC 1000 (Thermo Scientific) with solvent A consisting of 2% ACN in 0.5% acetic acid and solvent B consisting of 80% ACN in 0.5% acetic acid. The peptide mixture was gradient eluted into the QExactive mass spectrometer (Thermo Scientific) using the following gradient: a 5%-23% solvent B in 100 min, 23%-34% solvent B in 20 min, 34%-56% solvent B in 10 min, followed by 56%-100% solvent B in 20 min. The full scan was acquired with a resolution of 70,000 (@ *m*/*z* 200), a target value of 1e6 and a maximum ion time of 120 ms. After each full scan 10 HCD MS/MS scans were acquired using the following parameters: resolution 35,000 (@ *m*/*z* 200), isolation window of 1.5 *m*/*z*, target value of 1e5, maximum ion time of 250 ms, normalized collision energy (NCE) of 30, and dynamic exclusion of 30 s.

Raw mass spectrometry data were processed using Proteome Discoverer 2.1. Proteins and peptides were searched against the Mycobacterium tuberculosis H37Rv proteome using the Byonic with a protein score cut-off of 300, using the following settings: oxidized methionine (M), and deamidation (NQ) were selected as variable modifications, and carbamidomethyl (C) as fixed modifications; precursor mass tolerance 10 ppm; fragment mass tolerance 0.02 Da. Proteins identified with less than two unique peptides

were excluded from analysis. Bioinformatics analysis was performed with Perseus and Microsoft Excel. Student's t-test using Benjamini-Hochberg FDR cutoff was then used to identify proteins with differential abundance between bacterial strains.

REFERENCES FOR SI APPENDIX

1. Darwin KH, Ehrt S, Gutierrez-Ramos JC, Weich N, & Nathan CF (2003) The proteasome of Mycobacterium tuberculosis is required for resistance to nitric oxide. *Science* 302(5652):1963-1966.
2. Samanovic MI*, et al.* (2015) Proteasomal control of cytokinin synthesis protects Mycobacterium tuberculosis against nitric oxide. *Mol Cell* 57(6):984-994.
3. Gandotra S, Lebron MB, & Ehrt S (2010) The Mycobacterium tuberculosis proteasome active site threonine is essential for persistence yet dispensable for replication and resistance to nitric oxide. *PLoS Pathog* 6(8):e1001040.
4. Burns KE, Pearce MJ, & Darwin KH (2010) Prokaryotic ubiquitin-like protein provides a two-part degron to Mycobacterium proteasome substrates. *J Bacteriol* 192(11):2933-2935.
5. Chong YH*, et al.* (1994) Bacterial expression, purification of full length and carboxyl terminal fragment of Alzheimer amyloid precursor protein and their proteolytic processing by thrombin. *Life Sci* 54(17):1259-1268.
6. Miller VL & Mekalanos JJ (1988) A novel suicide vector and its use in construction of insertion mutations: osmoregulation of outer membrane proteins and virulence determinants in Vibrio cholerae requires toxR. *J Bacteriol* 170(6):2575-2583.
7. Rodionova IA*, et al.* (2015) Mycobacterial nicotinate mononucleotide adenylyltransferase: structure, mechanism, and implications for drug discovery. *J Biol Chem* 290(12):7693-7706.
8. Bardarov S*, et al.* (2002) Specialized transduction: an efficient method for generating marked and unmarked targeted gene disruptions in Mycobacterium tuberculosis, M. bovis BCG and M. smegmatis. *Microbiology* 148(Pt 10):3007-3017.
9. Stover CK*, et al.* (1991) New use of BCG for recombinant vaccines. *Nature* 351(6326):456-460.
10. Pham TT, Jacobs-Sera D, Pedulla ML, Hendrix RW, & Hatfull GF (2007) Comparative genomic analysis of mycobacteriophage Tweety: evolutionary insights and construction of compatible site-specific integration vectors for mycobacteria. *Microbiology* 153(Pt 8):2711-2723.
11. Ho SN, Hunt HD, Horton RM, Pullen JK, & Pease LR (1989) Site-directed mutagenesis by overlap extension using the polymerase chain reaction. *Gene* 77(1):51-59.
12. Hatfull GF & Jacobs WR (2000) *Molecular genetics of mycobacteria* (ASM Press, Washington, D.C.) pp xii, 363 p.
13. Cerda-Maira FA*, et al.* (2010) Molecular analysis of the prokaryotic ubiquitin-like protein (Pup) conjugation pathway in Mycobacterium tuberculosis. *Mol Microbiol* 77(5):1123-1135.
14. Tian J*, et al.* (2005) Mycobacterium tuberculosis appears to lack alpha-ketoglutarate dehydrogenase and encodes pyruvate dehydrogenase in widely separated genes. *Mol Microbiol* 57(3):859-868.
15. Festa RA*, et al.* (2010) Prokaryotic ubiquitin-like protein (Pup) proteome of Mycobacterium tuberculosis [corrected]. *PLoS One* 5(1):e8589.

16. Darwin KH, Lin G, Chen Z, Li H, & Nathan CF (2005) Characterization of a Mycobacterium tuberculosis proteasomal ATPase homologue. *Mol Microbiol* 55(2):561-571.
17. Chapman JR*, et al.* (2017) Phosphoproteomics of Fibroblast Growth Factor 1 (FGF1) Signaling in Chondrocytes: Identifying the Signature of Inhibitory Response. *Mol Cell Proteomics* 16(6):1126-1137.
18. Bhardwaj A, Yang Y, Ueberheide B, & Smith S (2017) Whole proteome analysis of human tankyrase knockout cells reveals targets of tankyrase-mediated degradation. *Nat Commun* 8(1):2214.